

Top-label calibration

Chirag Gupta, Aaditya K. Ramdas

chiragg@cmu.edu, aramd@cmu.edu

Carnegie Mellon University

July 20, 2021

Abstract

We study the problem of post-hoc calibration for multiclass classification, with an emphasis on histogram binning. Multiple works have focused on calibration with respect to the confidence of just the predicted class (or ‘top-label’). We find that the popular notion of confidence calibration [Guo et al., 2017] is not sufficiently strong—there exist predictors that are not calibrated in any meaningful way but are perfectly confidence calibrated. We propose a closely related (but subtly different) notion, *top-label calibration*, that accurately captures the intuition and simplicity of confidence calibration, but addresses its drawbacks. We formalize a histogram binning (HB) algorithm that reduces top-label multiclass calibration to the binary case, prove that it has clean theoretical guarantees without distributional assumptions, and perform a methodical study of its practical performance. Some prediction tasks require stricter notions of multiclass calibration such as class-wise or canonical calibration. We formalize appropriate HB algorithms corresponding to each of these goals. In experiments with deep neural nets, we find that our principled versions of HB are often better than temperature scaling, for both top-label and class-wise calibration. Code for this work will be made publicly available at <https://github.com/aigen/df-posthoc-calibration>.

Contents

1	Introduction	3
1.1	Related works	5
1.2	Post-hoc calibration setting	5
2	Distribution-free top-label calibration using histogram binning	6
2.1	Formal algorithm and theoretical guarantees	6
2.2	Top-label histogram binning adapts to class imbalanced datasets	8
2.3	Top-label histogram binning has lower TL-ECE than temperature scaling on CIFAR-10	9
2.4	Top-label histogram binning has higher TL-ECE than temperature scaling on CIFAR-100	10
3	Class-wise and canonical calibration using histogram binning	10
4	Conclusions and limitations	12
A	Distribution-free class-wise calibration using histogram binning	15
B	Binning schemes for canonical multiclass calibration	17
B.1	Sierpinski binning	18
B.2	Grid-style binning	19
B.3	Projection based histogram binning for canonical calibration	21
B.4	Experiments with the COVTYPE dataset	22
C	Proofs	24
C.1	Proof of Proposition 1	24
C.2	Proof of Theorem 1	24
C.3	Proof of Proposition 2	26
C.4	Proof of Theorem 2	26
D	Additional experimental details and results for Sections 1 and 2	28
D.1	Top-label calibration of COVTYPE-7	28
D.2	Top-label calibration of CIFAR-10 and CIFAR-100	28

1 Introduction

Calibration is a desirable property of validity for probabilistic predictions on a categorical outcome. For example, consider a meteorologist who claims that it is likely to rain on a particular day with probability 0.7. The meteorologist would be considered calibrated [Dawid, 1982] when the following occurs: if 0.7 is predicted on D different days of the year, then it indeed rains on roughly $0.7D$ of those days (and the same holds for other probabilities). In the same sense, an ML classification model would be considered more reliable if it makes calibrated probabilistic predictions for the classes [Platt, 1999, Zadrozny and Elkan, 2001]. A popular notion of calibration in multiclass classification settings is a simple ‘one-dimensional’ reduction to binary calibration proposed by Guo et al. [2017], called confidence calibration, which we recap below.

Let \mathcal{X} and $[L] := \{1, 2, \dots, L\}$ denote the feature and label spaces respectively. Consider a random point (X, Y) drawn from some distribution P over $\mathcal{X} \times [L]$. Let $c : \mathcal{X} \rightarrow [L]$ denote a classifier and $h : \mathcal{X} \rightarrow [0, 1]$ a function that provides a confidence score associated with the predicted class $c(X)$. The predictor (c, h) is said to be confidence calibrated (for P) if $P(Y = c(X) \mid h(X)) = h(X)$. In other words, the fraction of instances where the predicted top label is correct, when the confidence $h(X)$ is $p \in [0, 1]$, approximately equals p . It is common to measure the confidence-miscalibration of (c, h) using the expected-calibration-error (conf-ECE):

$$\text{conf-ECE}(c, h) := \mathbb{E}_X |P(Y = c(X) \mid h(X)) - h(X)|. \quad (1)$$

While confidence calibration is a reasonable minimum requirement, it is far from sufficient. Confidence calibration merges predictions with the same value of $h(X)$ across all classes; this merging can lead to predictors that have low conf-ECE but are not calibrated in any meaningful way.

Example 1 (Low conf-ECE does not imply meaningful calibration). We construct a predictor which is clearly miscalibrated but has conf-ECE = 0. Suppose the feature space is $\mathcal{X} = \{a, b\}$ and $P(X = a) = P(X = b) = 0.5$. Consider a predictor (c, h) with class predictions $c(a) = 1$, $c(b) = 2$, and confidence values $h(a) = h(b) = 0.6$. Let the true probabilities for the predicted class be $P(Y = 1 \mid X = a) = 0.2$ and $P(Y = 2 \mid X = b) = 1.0$. Observe that no matter what X is, the predicted probability of the top-label is 0.6, whereas the true probability is either 0.2 or 1.0. Despite this, the conf-ECE of (c, h) is 0 since $P(Y = c(X) \mid h(X) = 0.6) = 0.5 P(Y = 1 \mid X = a) + 0.5 P(Y = 2 \mid X = b) = 0.5(0.2 + 1) = 0.6$.

The reason for this strange behavior is that the probability $P(Y = c(X) \mid h(X))$ is not interpretable from a decision-making perspective. In practice, we always report both $c(X)$ and $h(X)$, and thus it is more reasonable to consider the conditional probability $P(Y = c(X) \mid c(X), h(X))$. Based on this understanding, we say that (c, h) is *top-label calibrated* if

$$P(Y = c(X) \mid h(X), c(X)) = h(X).$$

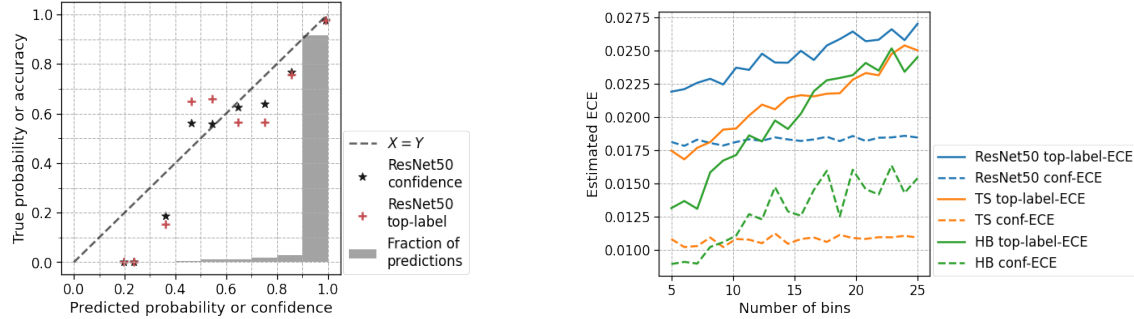
See the last paragraph of Section 1.1 for a disambiguating remark. Define the top-label-ECE as

$$\text{TL-ECE}(c, h) := \mathbb{E}_X |P(Y = c(X) \mid c(X), h(X)) - h(X)|. \quad (2)$$

The predictor in Example 1 has $\text{TL-ECE}(c, h) = 0.4$, revealing its miscalibration. The following proposition, proved in Appendix C, shows that TL-ECE is always higher than conf-ECE.

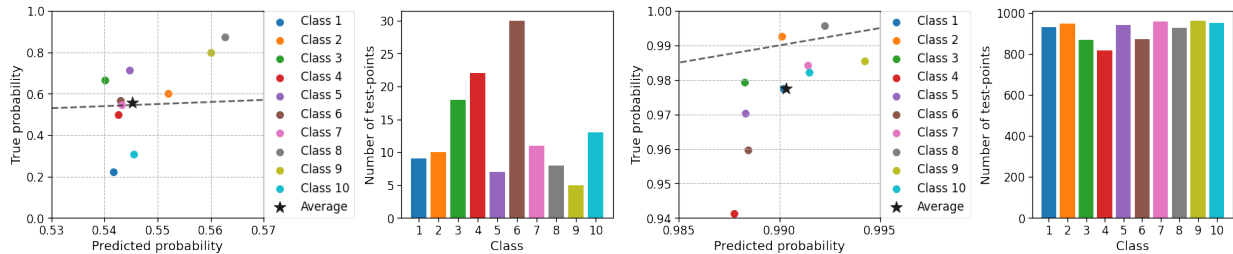
Proposition 1. *For any predictor (c, h) , $\text{conf-ECE}(c, h) \leq \text{TL-ECE}(c, h)$.*

In practice, more benign versions of Example 1 occur, where conf-ECE is not completely meaningless, but can be misleading. Figure 1 illustrates this through the (test-time) performance of a ResNet50 model [He et al., 2016] on the CIFAR-10 dataset [Krizhevsky, 2009]. Figure 1a is a confidence reliability diagram [Guo et al., 2017, Niculescu-Mizil and Caruana, 2005], constructed as follows. First, the $h(X)$ values on the test set are ‘binned’ into one of $B = 10$ bins $[0, 0.1), [0.1, 0.2), \dots, [0.9, 1]$, depending on the interval to which $h(X)$ belongs. The barplot in Figures 1a indicates the fraction of $h(X)$ values that belong to each bin; nearly 92% points belong to bin $[0.9, 1]$ and no points belong to bin $[0, 0.1)$. Next, for every bin b , the plugin estimate of $\text{acc}_b = P(Y = c(X) \mid h(X) \in \text{Bin } b)$ is plotted against the plugin estimate of $\text{conf}_b = \mathbb{E}[h(X) \mid h(X) \in \text{Bin } b]$. This forms the confidence reliability diagram (\star markers in Figure 1a).



(a) Confidence reliability diagram (points marked ★) and top-label reliability diagram (points marked +) for a pre-temperature scaling ResNet50 model. The confidence reliability diagram (mistakenly) suggests better calibration, unlike the top-label reliability diagram.

(b) Conf-ECE and TL-ECE estimates of base ResNet50 model, temperature scaled (TS) model, and histogram binning (HB) model as the number of bins is varied. Binning is competitive with temperature scaling when assessing TL-ECE (green/orange solid curves), and appears to have lower TL-ECE when the number of bins is small.



(c) Class-wise and zoomed-in version of Figure 1a for bin 6 (left) and bin 10 (right). The markers ★ are in the same position as Figure 1a, and denote the average predicted and true probabilities. The colored points denote the predicted and true probabilities when seen class-wise. The histograms show the number of test points per class in bins 6 and 10.

Figure 1: Confidence reliability diagrams and conf-ECE scores underestimate the effective miscalibration of a ResNet50 model on CIFAR-10.

The top-label reliability diagram assesses reliability when further conditioning on the predicted class and thus there are $L = 10$ different top-label reliability diagrams; in order to make a comparison to confidence calibration, we estimate the average miscalibration across classes,

$$\Delta_b := \sum_{l \in [L]} P(c(X) = l \mid h(X) \in \text{Bin } b) |P(Y = c(X) \mid c(X) = l, h(X) \in \text{Bin } b) - \mathbb{E}[h(X) \mid c(X) = l, h(X) \in \text{Bin } b]|,$$

and plot $(\text{conf}_b, \text{conf}_b + \Delta_b)$ if $\text{acc}_b > \text{conf}_b$; $(\text{conf}_b, \text{conf}_b - \Delta_b)$ otherwise (these are the + markers in Figure 1a). We find that there is a visible increase in miscalibration when going from confidence calibration to top-label calibration. To understand why this change occurs, let us zoom into bin 6 ($h(X) \in [0.5, 0.6)$) and bin 10 ($h(X) \in [0.9, 1.0]$). Figure 1c displays the class-wise top-label reliability diagrams for these bins. Note that for bin 6, the ★ marker is nearly on the $X = Y$ line, indicating that the overall accuracy matches the overall confidence. However, the true accuracy when class 1 was predicted is ≈ 0.2 and the true accuracy when class 8 was predicted is ≈ 0.9 (a very similar scenario to Example 1). For bin 10, the ★ marker indicates a miscalibration of ≈ 0.01 ; however, when class 4 was predicted (roughly 8% of all test-points) the miscalibration is ≈ 0.05 .

Figure 1b displays the aggregate effect of the above phenomenon (across bins and classes) through binned estimates of the conf-ECE and TL-ECE. This plot also displays the ECE estimates when the base model is recalibrated using temperature scaling [Guo et al., 2017] and histogram binning [Gupta and Ramdas, 2021, Zadrozny and Elkan, 2001]. Since ECE estimates depend on the number of bins B , we varied B in the range $[5, 25]$ to obtain unambiguous conclusions. The ECE estimate increases with B since (a) discretization through binning leads to underestimation of the ECE and (b) the plugin estimator is biased upwards [Bröcker, 2012, Kumar et al., 2019, Roelofs et al., 2020, Widmann et al., 2019]. We find that the TL-ECE of the pre-

and post-temperature scaling model is significantly higher than the conf-ECE across all values of B . For example, when $B = 15$, we observe that the TL-ECE of the temperature scaled ResNet model is nearly double its conf-ECE (going from ≈ 0.011 to ≈ 0.022). Further, while histogram binning appears worse than temperature scaling when assessing conf-ECE, it performs comparable or better than temperature scaling when assessing TL-ECE. Section 2 discusses top-label histogram binning in further detail.

1.1 Related works

Issues with confidence calibration have been noticed before in other works [Kull et al., 2019, Nixon et al., 2020, Vaicenavicius et al., 2019, Widmann et al., 2019], but the proposed solution in each of these works has been to consider notions of calibration that require more than just the top-label to be calibrated. For example, Kull et al. [2019, Figure 1] observed that a wide ResNet is confidence calibrated on CIFAR-10, but makes underconfident predictions for a specific class (across all bins). The issue illustrated in Figure 1c is different: even within a single bin, the under- and over- confident predictions can cancel out to indicate lower calibration than there actually is. Thus while previous works have proposed to fix confidence calibration by optimizing class-wise calibration metrics [Kull et al., 2019, Kumar et al., 2019, Nixon et al., 2020, Zadrozny and Elkan, 2002] or canonical calibration metrics [Vaicenavicius et al., 2019, Widmann et al., 2019], our work continues to advocate for calibrating probabilities only for the predicted class, which may be sufficient in many domains. Nevertheless, in Section 3 we develop histogram binning for class-wise and canonical calibration.

Any kind of ECE estimation through binning (for continuous output methods) suffers from discretization error. There is a growing body of literature on addressing this through assessment of calibration using kernel based metrics [Vaicenavicius et al., 2019, Widmann et al., 2019, Zhang et al., 2020], metrics based on hypothesis tests of calibration [Gupta et al., 2021, Vaicenavicius et al., 2019], or adaptive binning techniques [Kumar et al., 2019, Nixon et al., 2020, Roelofs et al., 2020]. Any of these techniques can be adapted for top-label calibration.

The term conf-ECE was introduced by Kull et al. [2019]. Most works refer to conf-ECE as just ECE [Guo et al., 2017, Kumar et al., 2018, Mukhoti et al., 2020, Nixon et al., 2020]. However, some papers refer to conf-ECE as ‘top-label-ECE’ [Kumar et al., 2019, Zhang et al., 2020], resulting in two different terms for the same concept. We continue to call conf-ECE by its original name, and *our definition of top-label calibration and top-label ECE (2) is different from previous ones.*

1.2 Post-hoc calibration setting

This paper considers the standard recalibration or post-hoc calibration setting. We start with a fixed ‘pre-learned’ base model $\mathbf{g} : \mathcal{X} \rightarrow \Delta^{L-1}$, where \mathcal{X} denotes the feature space and Δ^{L-1} is the probability simplex in L dimensions. (To ease readability, we typically use boldface characters such as $\mathbf{g}, \mathbf{h}, \mathbf{Y}$ to denote elements of Δ^{L-1} or functions whose range is Δ^{L-1} .) The base model \mathbf{g} can correspond to a deep net, a random forest, or any 1-v-all (one-versus-all) binary classification model such as logistic regression. The base model is typically optimized for classification accuracy and may not be calibrated. The goal of post-hoc calibration is to use some given *calibration data* $\mathcal{D} = (X_1, Y_1), (X_2, Y_2), \dots, (X_n, Y_n) \in (\mathcal{X} \times [L])^n$, typically data on which \mathbf{g} was not learnt, to recalibrate \mathbf{g} . We use (X, Y) to denote a random point identically distributed as the test point. For theoretical analysis, we assume that \mathcal{D} is a fresh sample statistically independent of \mathbf{g} , and the (X_i, Y_i) ’s are independent and identically distributed as (X, Y) .

Our theoretical guarantees make no assumptions other than this i.i.d. assumption. Thus our guarantees hold even when the data-generating distribution is arbitrarily non-smooth. This is known as the distribution-free setting [Gupta et al., 2020]. In practice, \mathcal{D} is often the same as the validation data; if \mathcal{D} is used for hyperparameter tuning, early stopping, etc., then the i.i.d. assumption is violated.

Post-hoc calibration for multiclass classification can occur under four different paradigms, illustrated in Figure 2. Letting g_l denote the l ’th component of \mathbf{g} , we can derive a top-label class predictor $c : \mathcal{X} \rightarrow [L]$ and a top-label confidence predictor $g : \mathcal{X} \rightarrow [0, 1]$ given by

$$c(\cdot) = \arg \max_{l \in [L]} g_l(\cdot), \quad \text{and} \quad g(\cdot) = \max_{l \in [L]} g_l(\cdot), \quad (3)$$

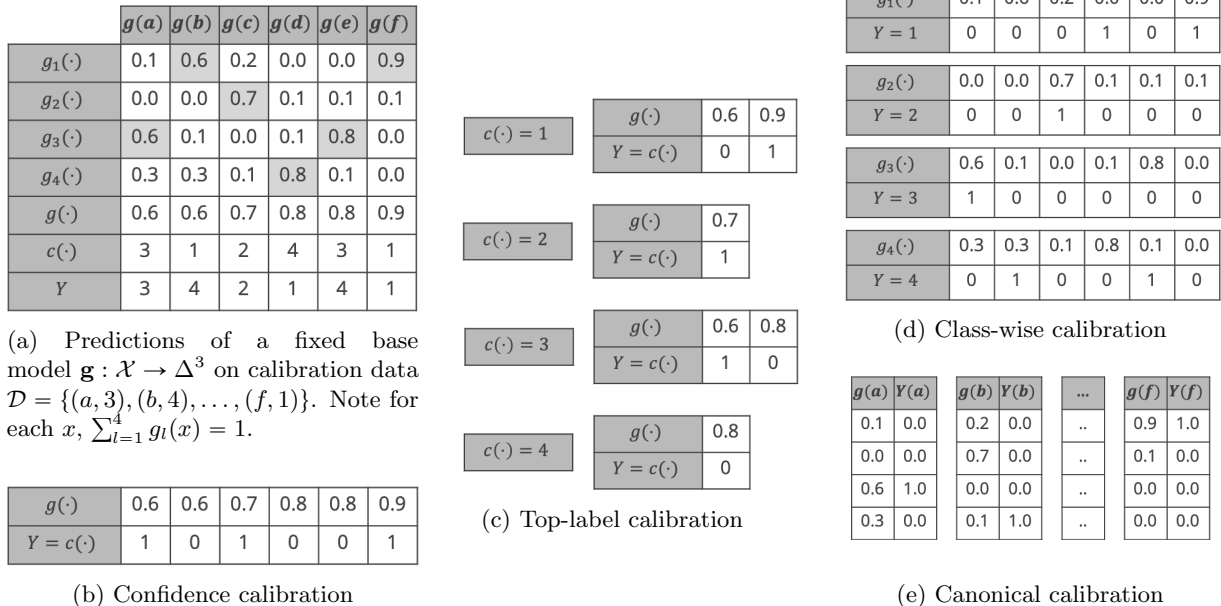


Figure 2: Paradigms of post-hoc multiclass calibration from most lenient (b) to most stringent (e). Plots (b–e) show the input for a calibration method that aims to achieve the corresponding notion. The numbers in these tables are derived from a fixed base classifier \mathbf{g} applied to the calibration data \mathcal{D} , given in plot (a). The top label is $c(\cdot)$, and $g(\cdot)$ is its confidence. Section 1.2 has further details.

assuming an arbitrary tie-breaking rule for the $\arg \max$. Confidence calibration (Figure 2b) cares only about g and the indicators $\mathbb{1}\{Y_i = c(X_i)\}$. Top-label calibration (Figure 2c) also focuses on g , but additionally requires access to the actual label predictions $c(X_i)$. This is used to produce one predictor for each label, denoted as h_1, h_2, \dots, h_L , but the final predictor for top-label calibration is a single h that predicts the h_l corresponding to the top-label: $h = h_{c(\cdot)}(\cdot)$. The class predictor c is not changed in this process, and thus the accuracy of (c, h) is the same as the accuracy of (c, g) . Class-wise calibration (Figure 2d, formally defined and discussed in Section 3) also produces h_1, h_2, \dots, h_L , but h_l is required to be calibrated whether or not l is the top-label. Unlike top-label calibration, a 1-v-all class-wise calibration method would use the g_l values on all n calibration points when learning h_l . Finally, the most stringent notion is canonical calibration (Figure 2e, formally defined and discussed in Section 3) where we think of the output as the canonical basis vector $\mathbf{Y}_i = \mathbf{e}_{Y_i}$ and aim for $\mathbf{h} : \mathcal{X} \rightarrow \Delta^{L-1}$ that (approximately) satisfies $\mathbb{E}[\mathbf{Y} \mid \mathbf{h}(X)] = \mathbf{h}(X)$.

2 Distribution-free top-label calibration using histogram binning

Histogram binning [Gupta and Ramdas, 2021, Zadrozny and Elkan, 2001] is a post-hoc calibration method where the base model and calibration data are used to partition \mathcal{X} into a number of ‘bins’, and the empirical distribution of the calibration Y_i values in each bin is used to recalibrate g . In this section, we formally describe histogram binning (HB) for top-label calibration and provide methodological insights through theory and experiments.

2.1 Formal algorithm and theoretical guarantees

As previewed in Section 1.2, to achieve top-label calibration, we start with a (miscalibrated) predictor $(c : \mathcal{X} \rightarrow [L], g : \mathcal{X} \rightarrow [0, 1])$. Then, the calibration data \mathcal{D} is divided into L different datasets $\{\mathcal{D}_l : l \in [L]\}$ based on the predicted class $c(X_i)$ for each point. The features in \mathcal{D}_l are the X_i ’s for which $c(X_i) = l$, and the labels are indicators of $Y_i = l$. Now for every $l \in [L]$, we calibrate g to $h_l : \mathcal{X} \rightarrow [0, 1]$ using \mathcal{D}_l and any binary calibration algorithm. The final predictor is defined as $h(\cdot) = h_{c(\cdot)}(\cdot)$. The top-label predictor $c(\cdot)$

Algorithm 1: Top-label histogram binning

Input: Base multiclass predictor \mathbf{g} , calibration data $\mathcal{D} = (X_1, Y_1), \dots, (X_n, Y_n)$
Hyperparameter: # points per bin $k \in \mathbb{N}$ (say 50), tie-breaking parameter $\delta > 0$ (say 10^{-10})
Output: Top-label calibrated predictor (c, h)

- 1 Define (c, g) from \mathbf{g} , using equation (3);
- 2 **for** $l \leftarrow 1$ **to** L **do**
- 3 $\mathcal{D}_l \leftarrow \{(X_i, \mathbb{1}\{Y_i = l\}) : c(X_i) = l\}$ and $n_l \leftarrow |\mathcal{D}_l|$;
- 4 $h_l \leftarrow \text{Binary-histogram-binning}(g, \mathcal{D}_l, \lfloor n_l/k \rfloor, \delta)$;
- 5 **end**
- 6 $h(\cdot) \leftarrow h_{c(\cdot)}(\cdot)$;
- 7 **return** (c, h) ;

does not change in this process. *Thus the accuracy of the top-label calibrated predictor is the same as that of the base predictor irrespective of the binary calibration algorithm used.*

Algorithm 1 describes the top-label calibration method formally using HB as the binary calibration algorithm. The function called in line 4 is Algorithm 2 of Gupta and Ramdas [2021]. The first argument in the call is the top-label confidence predictor, the second argument is the dataset to be used, the third argument is the number of bins to be used, and the fourth argument is a tie-breaking parameter (described shortly). While previous empirical works on HB fixed the *number of bins per class*, the analysis of Gupta and Ramdas [2021] suggests that a more principled way of choosing the number of bins is to fix the *number of points per bin*. This is parameter k of Algorithm 1. Given k , the number of bins is decided separately for every class as $\lfloor n_l/k \rfloor$ where n_l is the number of points predicted as class l . This choice is particularly relevant for top-label calibration since n_l can be highly non-uniform (we illustrate this empirically in Section 2.2). The tie-breaking parameter δ can be arbitrarily small (like 10^{-10}), and its significance is mostly theoretical—it is used to ensure that outputs of different bins are not exactly identical by chance, so that conditioning on a calibrated probability output is equivalent to conditioning on a bin; this leads to a cleaner theoretical guarantee.

HB recalibrates g to a piecewise constant function h that takes one value per bin. Consider a specific bin b ; the h value for this bin is computed as the average of the indicators $\{\mathbb{1}\{Y_i = c(X_i)\} : X_i \in \text{Bin } b\}$. This is an estimate of the ‘bias’ of the bin $P(Y = c(X) \mid X \in \text{Bin } b)$. A concentration inequality can then be used to bound the deviation between the estimate and the true bias to prove distribution-free calibration guarantees. In the forthcoming Theorem 1, we show high-probability and in-expectation bounds on the the TL-ECE of HB. Additionally, we show marginal and conditional top-label calibration bounds, defined next. These notions were proposed in the binary calibration setting by Gupta et al. [2020] and Gupta and Ramdas [2021]. In the definition below, \mathcal{A} refers to any algorithm that takes as input calibration data \mathcal{D} and an initial classifier \mathbf{g} to produce a top-label predictor c and an associated probability map h . Algorithm 1 is an example of \mathcal{A} .

Definition 1 (Marginal and conditional top-label calibration). Let $\varepsilon, \alpha \in (0, 1)$ be some given levels of approximation and failure respectively. An algorithm $\mathcal{A} : (\mathbf{g}, \mathcal{D}) \mapsto (c, h)$ is

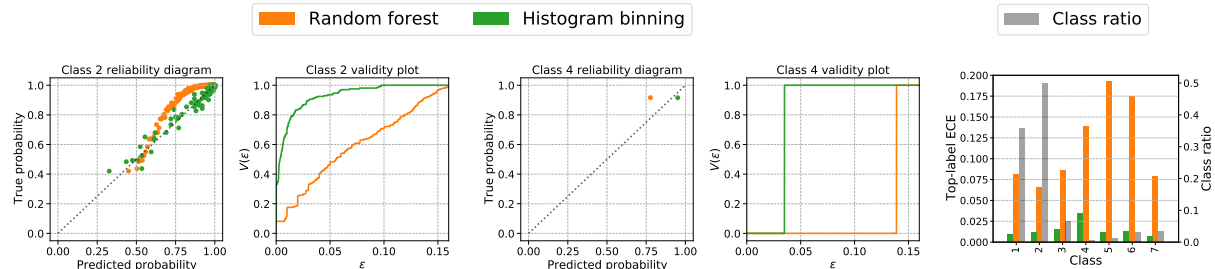
- (a) (ε, α) -marginally top-label calibrated if for every distribution P over $\mathcal{X} \times [L]$,

$$P\left(|P(Y = c(X) \mid c(X), h(X)) - h(X)| \leq \varepsilon\right) \geq 1 - \alpha. \quad (4)$$

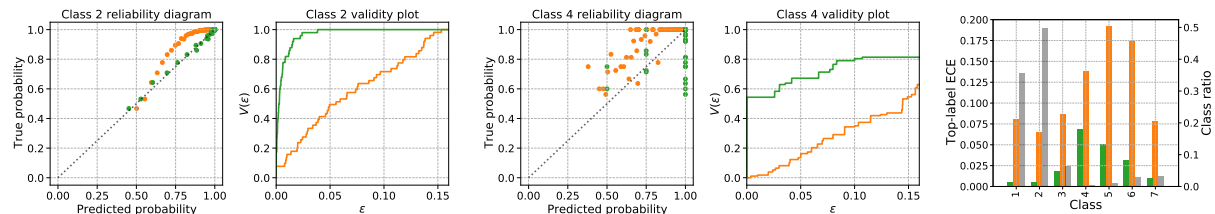
- (b) (ε, α) -conditionally top-label calibrated if for every distribution P over $\mathcal{X} \times [L]$,

$$P\left(\forall l \in [L], r \in \text{Range}(h), |P(Y = c(X) \mid c(X) = l, h(X) = r) - r| \leq \varepsilon\right) \geq 1 - \alpha. \quad (5)$$

To clarify, all probabilities are taken over the test point $(X, Y) \sim P$, the calibration data $\mathcal{D} \sim P^n$, and any other inherent algorithmic randomness in \mathcal{A} ; these are all implicit in $(c, h) = \mathcal{A}(\mathcal{D}, \mathbf{g})$. Marginal calibration asserts that with high probability, on average over the distribution of \mathcal{D}, X , $P(Y = c(X) \mid c(X), h(X))$ is



(a) Top-label histogram binning (Algorithm 1) with $k = 100$ points per bin. Class 4 has only 183 calibration points. Algorithm 1 adapts and uses only a single bin to ensure that the TL-ECE on class 4 is comparable to the TL-ECE on class 2. Overall, the random forest classifier has significantly higher TL-ECE for the least likely classes (4, 5, and 6), but the post-calibration TL-ECE using binning is quite uniform.



(b) Histogram binning with $B = 50$ bins for every class. Compared to Figure 3a, the post-calibration TL-ECE for the most likely classes decreases while the TL-ECE for the least likely classes increases.

Figure 3: Recalibration of a random forest using histogram binning on the class imbalanced COVTYPE-7 dataset (class 2 is roughly 100 times likelier than class 4). By ensuring a fixed number of calibration points per bin, Algorithm 1 obtains relatively uniform top-label calibration across classes (Figure 3a). In comparison, if a fixed number of bins are chosen for all classes, the performance deteriorates for the least likely classes (Figure 3b).

at most ε away from $h(X)$. In comparison, TL-ECE is the average of these deviations over X . Marginal calibration may be a more appropriate metric for calibration than TL-ECE if we are somewhat agnostic to probabilistic errors less than some fixed threshold ε (like 0.05). Conditional calibration is a strictly stronger definition that requires the deviation to be at most ε for every possible prediction (l, r) , including rare ones, not just on average over predictions. This may be relevant in medical settings where we want the prediction on every patient to be reasonably calibrated. Algorithm 1 satisfies the following calibration guarantees.

Theorem 1. Fix hyperparameters $\delta > 0$ (arbitrarily small) and points per bin $k \geq 2$, and assume $n_l \geq k$ for every $l \in [L]$. Then, for any $\alpha \in (0, 1)$, Algorithm 1 is (ε_1, α) -marginally and (ε_2, α) -conditionally top-label calibrated for

$$\varepsilon_1 = \sqrt{\frac{\log(2/\alpha)}{2(k-1)}} + \delta, \quad \text{and} \quad \varepsilon_2 = \sqrt{\frac{\log(2n/k\alpha)}{2(k-1)}} + \delta. \quad (6)$$

Further, for any distribution P over $\mathcal{X} \times [L]$, $P(\text{TL-ECE}(c, h) \leq \varepsilon_2) \geq 1 - \alpha$, and $\mathbb{E}[\text{TL-ECE}(c, h)] \leq \sqrt{1/2k} + \delta$.

The proof in Appendix C is a multiclass top-label adaption of the guarantee in the binary setting by Gupta and Ramdas [2021]. The $\tilde{O}(1/\sqrt{k})$ dependence of the bound relies on Algorithm 1 delegating at least k points to every bin. Since δ can be chosen to be arbitrarily small, setting $k = 50$ gives roughly $\mathbb{E}_{\mathcal{D}}[\text{TL-ECE}(h)] \leq 0.1$. Based on this, we suggest setting $k \in [50, 150]$ in practice.

2.2 Top-label histogram binning adapts to class imbalanced datasets

The principled methodology of fixing the number of points per bin reaps practical benefits. Figure 3 illustrates this through the performance of HB for the class imbalanced COVTYPE-7 dataset [Blackard and Dean, 1999]

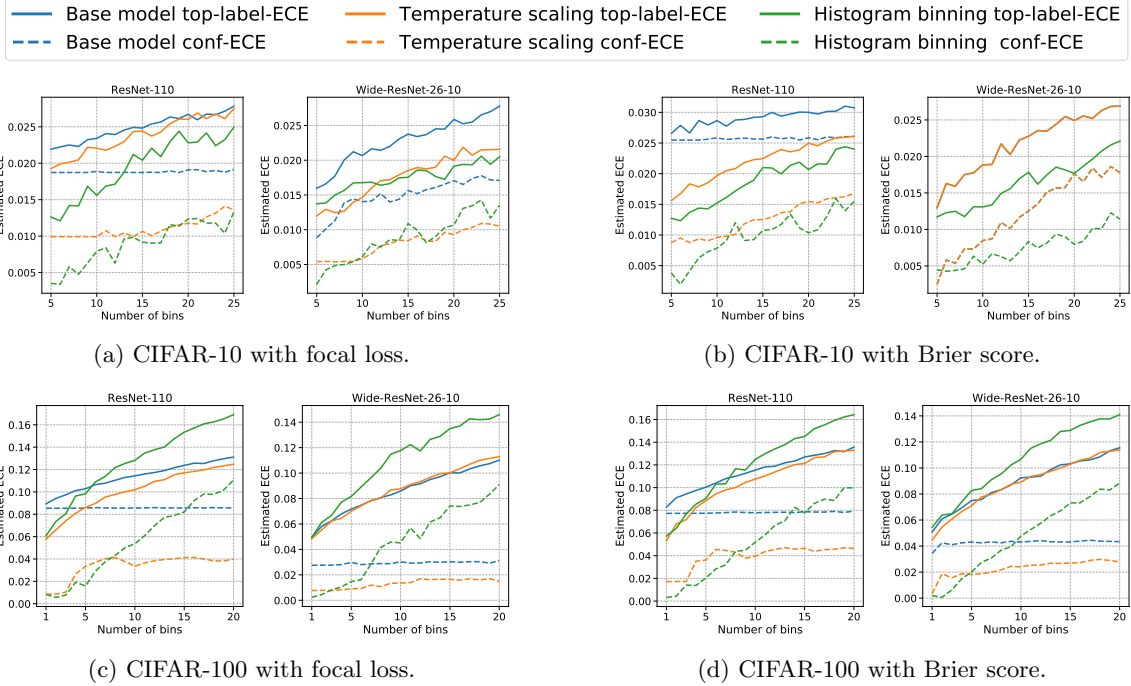


Figure 4: ECE of histogram binning and temperature scaling with deep nets on CIFAR-10 and CIFAR-100. Histogram binning has lower estimated TL-ECE on CIFAR-10, but higher on CIFAR-100. Similar plots with ResNet-50 and DenseNet-121 are presented in Appendix D.

with class ratio approximately 36% for class 1 and 49% for class 2. The entire dataset has 581012 points which is divided into train-test in the ratio 70:30. Then, 10% of the training points are held out for calibration ($n = |\mathcal{D}| = 40671$). The base classifier is a random forest (RF) trained on the remaining training points (it achieves around 95% test accuracy). The RF is then recalibrated using HB. The top-label reliability diagrams in Figure 3a illustrate that the original RF (in orange) is *underconfident* on both the most likely and least likely classes. Additional figures in Appendix D show that the RF is always underconfident no matter which class is predicted as the top-label. HB (in green) recalibrates the RF effectively across all classes. Validity plots [Gupta and Ramdas, 2021] estimate how the LHS of condition (4), denoted as $V(\varepsilon)$, varies with ε . We observe that for all ε , $V(\varepsilon)$ is higher for HB. The rightmost barplot compares the estimated TL-ECE for all classes, and also shows the class proportions. While the original RF is significantly miscalibrated for the less likely classes, HB has a more uniform miscalibration across classes. Figure 3b considers a slightly different HB algorithm where the number of points per class is not adapted to the number of times the class is predicted, but is fixed beforehand (this corresponds to replacing $\lfloor n_i/k \rfloor$ in line 4 of Algorithm 1 with a fixed $B \in \mathbb{N}$). While even in this setting there is a drop in the TL-ECE compared to the RF model, the final profile is less uniform compared to fixing the number of points per bin.

2.3 Top-label histogram binning has lower TL-ECE than temperature scaling on CIFAR-10

Figures 4a and 4b compare the test-time performance of HB to the popular post-hoc calibration method of temperature scaling (TS) proposed by Guo et al. [2017], with deep neural networks as the base models, and CIFAR-10 [Krizhevsky, 2009] as the dataset. We used the base models trained by Mukhoti et al. [2020] on the following architectures: ResNet-50, Resnet-110 [He et al., 2016], Wide-ResNet-26-10 [Zagoruyko and Komodakis, 2016], and DensetNet-121 [Huang et al., 2017].¹ Mukhoti et al. [2020] noted that using the loss

¹The models were obtained from www.robots.ox.ac.uk/~viveka/focal_calibration/ and used along with the code at https://github.com/torrvision/focal_calibration to obtain base predictions.

function as the Brier score, or their proposed focal loss, leads to the best performance pre- and post- TS. Our experiment uses the exact base models that lead to the numbers in Table 1 of their paper (corresponding to the columns ‘Brier Loss’ and ‘FLSD-53’), and the same calibration data that was used for TS was also used for HB. We did not perform any additional tuning, and our results are thus relatively free of selection biases.

The calibration data for CIFAR-10 has roughly 500 points for each of the 10 classes. Since there is no class imbalance, and to have unambiguous conclusions, we used a fixed number of bins per-class for HB (this is contradictory to Algorithm 1, but we do so to ease comparison of results to TS). We ranged the number of bins range from 5 to 25. The ECE of the base model and TS was estimated using fixed-width binning, with the same number of bins as HB. Fixed-width binning gives TS a slight advantage since if adaptive/uniform-mass bins are used, the conf-ECE estimate of TS increases; see Table F.1 [Mukhoti et al., 2020]. No further binning is needed for estimating the ECE of HB since it already provides a discrete output (binning will only decrease the ECE estimate).

As previewed in Section 1, Figures 4a and 4b indicate that (a) the TL-ECE estimate of TS is significantly higher than the conf-ECE estimate, and (b) HB performs better than TS with respect to the TL-ECE estimates, across different numbers of bins. In all our experiments, the temperature parameter of TS was chosen to give optimal conf-ECE on the calibration data (following Mukhoti et al. [2020]). We hypothesized that if T is chosen to optimize TL-ECE on the calibration data, the testing TL-ECE would improve, but in our experiments, the testing TL-ECE actually worsened — these results are thus not presented. In Appendix D we define the maximum calibration error metric (MCE) metric [Naeini et al., 2015] with respect to top-label calibration, and compare HB and TS based on the MCE. We find that the relative performance of HB for MCE is drastically better than TS. Next, we present a negative result for histogram binning.

2.4 Top-label histogram binning has higher TL-ECE than temperature scaling on CIFAR-100

CIFAR-100 is a balanced dataset with 100 classes and 5000 points for validation/calibration (as per the default splits). Due to random subsampling, the validation split we used had one of the classes predicted as the top-label only 31 times. Thus, based on our theory, we do not expect HB to have small TL-ECE. This is confirmed by the plots in Figures 4c and 4d (the experimental setup is same as CIFAR-10). We observe that HB has higher estimated TL-ECE than TS for most values of the number of bins (and typically also higher TL-ECE than the base model). However in Section 3 we show that for class-wise calibration, HB performs better than TS on CIFAR-100. This is because in the class-wise setting, 5000 points are available for recalibration, which is sufficient for HB.

The deterioration in performance of HB when few calibration points are available was also observed in the binary setting by Gupta and Ramdas [2021, Appendix C]. Niculescu-Mizil and Caruana [2005] noted in the conclusion of their paper that Platt scaling [Platt, 1999], which is closely related to TS, performs well when the data is small, but another nonparametric binning method, isotonic regression [Zadrozny and Elkan, 2002] performs better when enough data is available. Kull et al. [2019, Section 4.1] compared HB to other calibration techniques for class-wise calibration on 21 UCI datasets, and found that HB performs the worst. On inspecting the UCI repository, we found that most of the datasets they used had fewer than 5000 (total) data points, and many contain fewer than 500.

Overall, comparing our results to previous empirical studies, we believe that if sufficiently many points are available for recalibration, or the number of classes is small, then HB performs quite well. To be more precise, we expect HB to be competitive if at least 200 points per class can be held out for recalibration, and the number of points per bin is at least $k \geq 20$.

3 Class-wise and canonical calibration using histogram binning

Domains such as medicine may require that predictions for important classes be calibrated even if they are not predicted to be the top-label. To this end, class-wise calibration [Zadrozny and Elkan, 2002] and canonical calibration [Vaicenavicius et al., 2019] require the full L -dimensional prediction vector to be calibrated. A predictor $\mathbf{h} = (h_1, h_2, \dots, h_L)$ is said to be class-wise calibrated if for every $l \in [L]$, $P(Y = l | h_l(X)) = h_l(X)$,

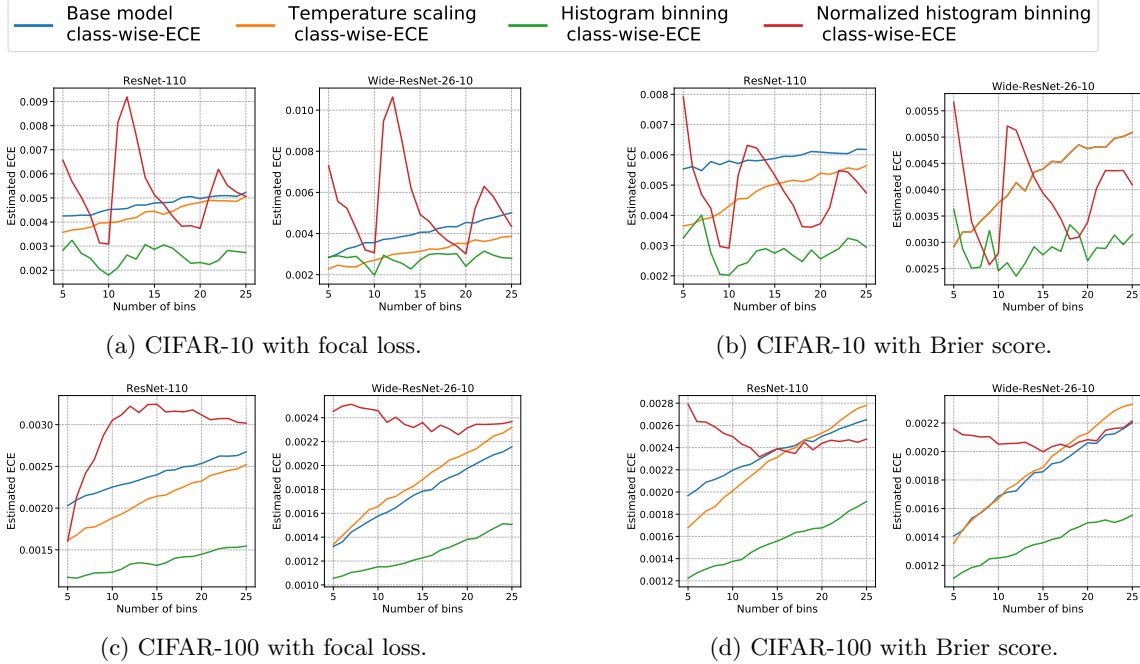


Figure 5: CW-ECE of non-normalized histogram binning, normalized histogram binning, and temperature scaling, with deep nets on CIFAR-10 and CIFAR-100. Non-normalized histogram binning performs the best overall. Plots with ResNet-50 and DenseNet-121 are presented in Appendix A.

and canonically calibrated if $\mathbb{E}[\mathbf{Y} \mid \mathbf{h}(X)] = \mathbf{h}(X)$ (see Section 1.2 for notation). Canonical calibration implies class-wise calibration.

Proposition 2. *If $\mathbb{E}[\mathbf{Y} \mid \mathbf{h}(X)] = \mathbf{h}(X)$, then for every $l \in [L]$, $P(Y = l \mid h_l(X)) = h_l(X)$.*

The proof in Appendix C is straightforward, but the statement above is illuminating, because there exist predictors that are class-wise calibrated but not canonically calibrated [Vaicenavicius et al., 2019, Example 1]. A measure of the class-wise calibration of (c, \mathbf{h}) is the class-wise-ECE [Kull et al., 2019], also called marginal-ECE [Kumar et al., 2019] or static-ECE [Nixon et al., 2020]:

$$\text{CW-ECE}(c, \mathbf{h}) := L^{-1} \sum_{l=1}^L \mathbb{E}_X |P(Y = l \mid h_l(X)) - h_l(X)|. \quad (7)$$

A common way to achieve class-wise calibration is to use a binary calibration algorithm in a 1-v-all paradigm, as illustrated in Figure 2d, to learn L predictors h_1, h_2, \dots, h_L . The predictors are then normalized so that the final prediction sums to one: $h_l^{\text{norm}}(\cdot) := h_l(\cdot) / \sum_{u=1}^L h_u(\cdot)$. While the normalization makes sense for interpretability of the prediction, it is not required by the class-wise calibration condition or the CW-ECE formulation, both of which assess the h_l 's individually. In Appendix A, we formally state a *non-normalized* class-wise histogram binning algorithm and show that it satisfies calibration guarantees similar to Theorem 1. We were unable to derive such guarantees for normalized HB. We hypothesized that normalization could hurt the performance of HB in practice as well, and found that this is indeed the case. Figure 5 presents estimates of the CW-ECE for CIFAR-10 and CIFAR-100 with deep neural nets (under the same setup as Sections 2.3, 2.4). Non-normalized 1-v-all HB performs better than temperature scaling in all our experiments, and normalized HB performs worse than even the base model. Guo et al. [2017] and Kull et al. [2019] have also noted such negative results for normalized HB. Our experiments reveal that these negative results are not inherent to HB but are simply due to an incorrect normalization step.

For canonical calibration, we can surmise binning schemes that directly learn \mathbf{h} by partitioning the prediction space Δ^{L-1} into bins and estimating the distribution of \mathbf{Y} in each bin. A canonical calibration guarantee can be showed for such a binning scheme using multinomial concentration [Podkopaev and Ramdas, 2021, Section 3.1]. However, since $\text{Vol}(\Delta^{L-1}) = 2^{\Theta(L)}$, there will either be a bin whose volume is $2^{\Omega(L)}$

(meaning that \mathbf{h} would not be sharp), or the number of bins will be $2^{\Omega(L)}$, entailing $2^{\Omega(L)}$ requirements on the sample complexity — a ‘curse of dimensionality’. Nevertheless, in Appendix B, we propose some binning schemes which could work if L is small.

4 Conclusions and limitations

Confidence calibration is an intuitive one-dimensional reduction of multiclass calibration, but is not interpretable from a decision-making perspective. Top-label calibration captures the simplicity of confidence calibration, but addresses its issues. Histogram binning is a principled method for achieving top-label and class-wise calibration that satisfies distribution-free calibration guarantees. In contrast, Gupta et al. [2020] showed in the binary setting that continuous output methods such as temperature scaling cannot satisfy distribution-free calibration. Our theory provides a principled way of choosing the number of points per bin in histogram binning. When this choice is practically feasible (i.e. enough calibration points are available), histogram binning shows promising practical performance. Finally, we also note that since histogram binning is a discrete output method, it does not require complicated techniques for ECE estimation; simple plugin estimates are sufficient.

Limitations. Post-hoc calibration requires keeping aside a fresh, representative dataset, that was not used for training. If this dataset is too small, the resulting calibration guarantee can be too weak to be meaningful in practice. Further, if the test data distribution shifts in significant ways, additional corrections may be needed to recalibrate [Gupta et al., 2020, Podkopaev and Ramdas, 2021]. A well calibrated classifier is not necessarily an accurate or a fair one, and vice versa [Kleinberg et al., 2017]. Deploying calibrated models in critical applications like medicine, criminal law, banking, etc. does not preclude the possibility of the model being frequently wrong or unfair.

Acknowledgements

This work used the Extreme Science and Engineering Discovery Environment (XSEDE), which is supported by National Science Foundation grant number ACI-1548562 [Towns et al., 2014]. Specifically, it used the Bridges-2 system, which is supported by NSF award number ACI-1928147, at the Pittsburgh Supercomputing Center (PSC). CG would like to thank Saurabh Garg and Youngseog Chung for interesting discussions, and Viveka Kulharia for help with the focal calibration repository (https://github.com/torrvision/focal_calibration).

References

- Jock A Blackard and Denis J Dean. Comparative accuracies of artificial neural networks and discriminant analysis in predicting forest cover types from cartographic variables. *Computers and electronics in agriculture*, 24(3):131–151, 1999.
- Leo Breiman, Jerome H Friedman, Richard A Olshen, and Charles J Stone. *Classification and regression trees*. Routledge, 2017.
- Jochen Bröcker. Estimating reliability and resolution of probability forecasts through decomposition of the empirical score. *Climate dynamics*, 39(3-4):655–667, 2012.
- A Philip Dawid. The well-calibrated Bayesian. *Journal of the American Statistical Association*, 77(379):605–610, 1982.
- Luc Devroye. The equivalence of weak, strong and complete convergence in L_1 for kernel density estimates. *The Annals of Statistics*, 11(3):896–904, 1983.
- Luc Devroye. Automatic pattern recognition: A study of the probability of error. *IEEE Transactions on pattern analysis and machine intelligence*, 10(4):530–543, 1988.

- Louis Gordon and Richard A Olshen. Almost surely consistent nonparametric regression from recursive partitioning schemes. *Journal of Multivariate Analysis*, 15(2):147–163, 1984.
- Chuan Guo, Geoff Pleiss, Yu Sun, and Kilian Q. Weinberger. On calibration of modern neural networks. In *International Conference on Machine Learning*, 2017.
- Chirag Gupta and Aaditya Ramdas. Distribution-free calibration guarantees for histogram binning without sample splitting. In *International Conference on Machine Learning*, 2021.
- Chirag Gupta, Aleksandr Podkopaev, and Aaditya Ramdas. Distribution-free binary classification: prediction sets, confidence intervals and calibration. In *Advances in Neural Information Processing Systems*, 2020.
- Kartik Gupta, Amir Rahimi, Thalaiyasingam Ajanthan, Thomas Mensink, Cristian Sminchisescu, and Richard Hartley. Calibration of neural networks using splines. In *International Conference on Learning Representations*, 2021.
- Kaiming He, Xiangyu Zhang, Shaoqing Ren, and Jian Sun. Deep residual learning for image recognition. In *Proceedings of the IEEE Conference on Computer Vision and Pattern Recognition*, 2016.
- Gao Huang, Zhuang Liu, Laurens Van Der Maaten, and Kilian Q Weinberger. Densely connected convolutional networks. In *Proceedings of the IEEE Conference on Computer Vision and Pattern Recognition*, 2017.
- Jon Kleinberg, Sendhil Mullainathan, and Manish Raghavan. Inherent trade-offs in the fair determination of risk scores. In *Innovations in Theoretical Computer Science*, 2017.
- Alex Krizhevsky. Learning multiple layers of features from tiny images. *Technical Report, University of Toronto*, 2009.
- Meelis Kull, Miquel Perello-Nieto, Markus Kängsepp, Hao Song, and Peter Flach. Beyond temperature scaling: Obtaining well-calibrated multiclass probabilities with Dirichlet calibration. In *Advances in Neural Information Processing Systems*, 2019.
- Ananya Kumar, Percy S Liang, and Tengyu Ma. Verified uncertainty calibration. In *Advances in Neural Information Processing Systems*, 2019.
- Aviral Kumar, Sunita Sarawagi, and Ujjwal Jain. Trainable calibration measures for neural networks from kernel mean embeddings. In *International Conference on Machine Learning*, 2018.
- Gábor Lugosi and Andrew Nobel. Consistency of data-driven histogram methods for density estimation and classification. *Annals of Statistics*, 24(2):687–706, 1996.
- Jishnu Mukhoti, Viveka Kulharia, Amartya Sanyal, Stuart Golodetz, Philip HS Torr, and Puneet K Dokania. Calibrating deep neural networks using focal loss. In *Advances in Neural Information Processing Systems*, 2020.
- Mahdi Pakdaman Naeini, Gregory Cooper, and Milos Hauskrecht. Obtaining well calibrated probabilities using Bayesian binning. In *AAAI Conference on Artificial Intelligence*, 2015.
- Alexandru Niculescu-Mizil and Rich Caruana. Predicting good probabilities with supervised learning. In *International Conference on Machine Learning*, 2005.
- Jeremy Nixon, Michael W Dusenberry, Linchuan Zhang, Ghassen Jerfel, and Dustin Tran. Measuring calibration in deep learning. *arXiv preprint arXiv:1904.01685*, 2020.
- Andrew Nobel. Histogram regression estimation using data-dependent partitions. *The Annals of Statistics*, 24(3):1084–1105, 1996.
- John C. Platt. Probabilistic outputs for support vector machines and comparisons to regularized likelihood methods. In *Advances in Large Margin Classifiers*, pages 61–74. MIT Press, 1999.

- Aleksandr Podkopaev and Aaditya Ramdas. Distribution-free uncertainty quantification for classification under label shift. In *Uncertainty in Artificial Intelligence*, 2021.
- Jian Qian, Ronan Fruit, Matteo Pirota, and Alessandro Lazaric. Concentration inequalities for multinoulli random variables. *arXiv preprint arXiv:2001.11595*, 2020.
- Rebecca Roelofs, Nicholas Cain, Jonathon Shlens, and Michael C Mozer. Mitigating bias in calibration error estimation. *arXiv preprint arXiv:2012.08668*, 2020.
- J. Towns, T. Cockerill, M. Dahan, I. Foster, K. Gaither, A. Grimshaw, V. Hazlewood, S. Lathrop, D. Lifka, G. D. Peterson, R. Roskies, J. Scott, and N. Wilkins-Diehr. XSEDE: Accelerating Scientific Discovery. *Computing in Science & Engineering*, 16(5):62–74, 2014.
- Juozas Vaicenavicius, David Widmann, Carl Andersson, Fredrik Lindsten, Jacob Roll, and Thomas B Schön. Evaluating model calibration in classification. In *International Conference on Artificial Intelligence and Statistics*, 2019.
- Tsachy Weissman, Erik Ordentlich, Gadiel Seroussi, Sergio Verdu, and Marcelo J Weinberger. Inequalities for the L1 deviation of the empirical distribution. *Hewlett-Packard Labs, Tech. Rep*, 2003.
- David Widmann, Fredrik Lindsten, and Dave Zachariah. Calibration tests in multi-class classification: a unifying framework. In *Advances in Neural Information Processing Systems*, 2019.
- Bianca Zadrozny and Charles Elkan. Obtaining calibrated probability estimates from decision trees and naive Bayesian classifiers. In *International Conference on Machine Learning*, 2001.
- Bianca Zadrozny and Charles Elkan. Transforming classifier scores into accurate multiclass probability estimates. In *International Conference on Knowledge Discovery and Data Mining*, 2002.
- Sergey Zagoruyko and Nikos Komodakis. Wide residual networks. In *British Machine Vision Conference*, 2016.
- Jize Zhang, Bhavya Kailkhura, and T Han. Mix-n-match: Ensemble and compositional methods for uncertainty calibration in deep learning. In *International Conference on Machine Learning*, 2020.

Algorithm 2: Class-wise histogram binning

Input: Base multiclass predictor $\mathbf{g} : \mathcal{X} \rightarrow \Delta^{L-1}$, calibration data $\mathcal{D} = (X_1, Y_1), \dots, (X_n, Y_n)$
Hyperparameter: # points per bin $k_1, k_2, \dots, k_L \in \mathbb{N}^L$ (say each $k_l = 50$), tie-breaking parameter $\delta > 0$ (say 10^{-10})
Output: L class-wise calibrated predictors h_1, h_2, \dots, h_L

- 1 **for** $l \leftarrow 1$ **to** L **do**
- 2 $\mathcal{D}_l \leftarrow \{(X_i, \mathbb{1}\{Y_i = l\}) : i \in [n]\}$;
- 3 $h_l \leftarrow \text{Binary-histogram-binning}(g, \mathcal{D}_l, \lfloor n/k_l \rfloor, \delta)$;
- 4 **end**
- 5 **return** (h_1, h_2, \dots, h_L) ;

A Distribution-free class-wise calibration using histogram binning

We define marginal and conditional calibration for class-wise calibration, analogous to Definition 1, and state a histogram binning algorithm that is calibrated with respect to these notions. We also show bounds on the CW-ECE of the proposed algorithm (CW-ECE is defined in equation (7)).

A general algorithm \mathcal{A} for class-wise calibration takes as input calibration data \mathcal{D} and an initial classifier \mathbf{g} to produce an approximately class-wise calibrated predictor $\mathbf{h} : \mathcal{X} \rightarrow [0, 1]^L$. Recall that we denote the component functions of \mathbf{h} as h_1, h_2, \dots, h_L . In the same fashion, define the notation $\boldsymbol{\varepsilon} = (\varepsilon_1, \varepsilon_2, \dots, \varepsilon_L) \in (0, 1)^L$ and $\boldsymbol{\alpha} = (\alpha_1, \alpha_2, \dots, \alpha_L) \in (0, 1)^L$.

Definition 2 (Marginal and conditional class-wise calibration). Let $\boldsymbol{\varepsilon}, \boldsymbol{\alpha} \in (0, 1)^L$ be some given levels of approximation and failure respectively. An algorithm $\mathcal{A} : (\mathbf{g}, \mathcal{D}) \mapsto \mathbf{h}$ is

(a) $(\boldsymbol{\varepsilon}, \boldsymbol{\alpha})$ -marginally class-wise calibrated if for every distribution P over $\mathcal{X} \times [L]$ and for every $l \in [L]$

$$P\left(|P(Y = l | h_l(X)) - h_l(X)| \leq \varepsilon_l\right) \geq 1 - \alpha_l. \tag{8}$$

(b) $(\boldsymbol{\varepsilon}, \boldsymbol{\alpha})$ -conditionally class-wise calibrated if for every distribution P over $\mathcal{X} \times [L]$ and for every $l \in [L]$,

$$P\left(\forall r \in \text{Range}(h_l), |P(Y = l | h_l(X) = r) - r| \leq \varepsilon_l\right) \geq 1 - \alpha_l. \tag{9}$$

Definition 2 requires that each h_l is $(\varepsilon_l, \alpha_l)$ calibrated in the binary senses defined by Gupta et al. [2021, Definitions 1 and 2]. From Definition 2, we can also *uniform* bounds that hold simultaneously over every $l \in [L]$. Let $\alpha = \sum_{l=1}^L \alpha_l$ and $\varepsilon = \max_{l \in [L]} \varepsilon_l$. Then (8) implies

$$P\left(\forall l \in [L], |P(Y = l | h_l(X)) - h_l(X)| \leq \varepsilon\right) \geq 1 - \alpha, \tag{10}$$

and (9) implies

$$P\left(\forall l \in [L], r \in \text{Range}(h_l), |P(Y = l | h_l(X) = r) - r| \leq \varepsilon\right) \geq 1 - \alpha. \tag{11}$$

The choice of not including the uniformity over L in Definition 2 reveals the nature of our class-wise HB algorithm and the upcoming theoretical guarantees: (a) we learn the h_l 's separately for each l and do not combine the learnt functions in any way (such as normalization), (b) we do not combine the calibration inequalities for different $[L]$ in any other way other than a union bound. Thus the only way we can show (10) (or (11)) is by using a union bound over (8) (or (9)).

To achieve class-wise calibration using binary routines, we learn each component function h_l in a 1-v-all fashion. Algorithm 2 contains the pseudocode with the underlying routine as binary HB. To learn h_l , we use a dataset \mathcal{D}_l , which unlike top-label HB (Algorithm 1), contains X_i even if $c(X_i) \neq l$. However the Y_i is replaced with $\mathbb{1}\{Y_i = l\}$. The number of points per bin k_l can be different for different classes, but generally one would set $k_1 = \dots = k_L = k \in \mathbb{N}$. Larger values of k_l will lead to smaller ε_l and δ_l in the guarantees, at loss of sharpness since the number of bins $\lfloor n/k_l \rfloor$ would be smaller.

We now state the distribution-free calibration guarantees satisfied by Algorithm 2.

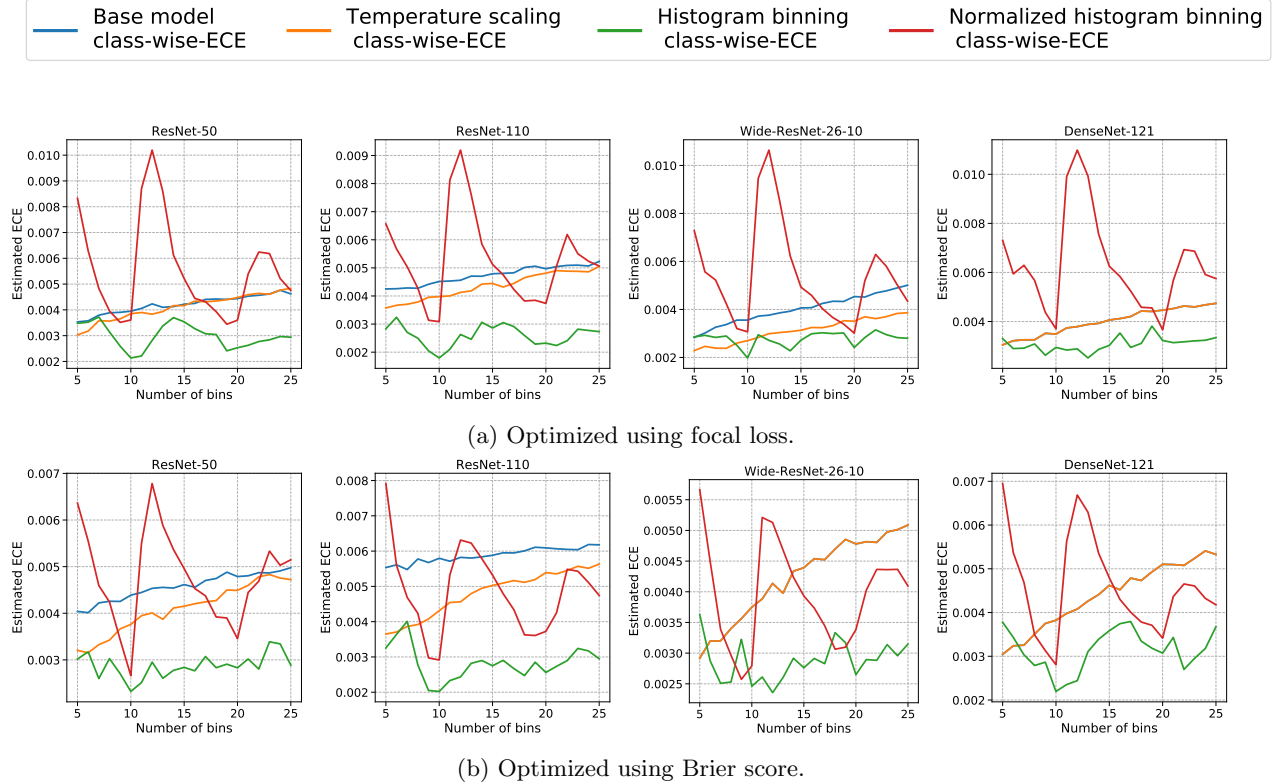


Figure 6: CW-ECE of histogram binning (HB) and temperature scaling (TS) with deep nets on CIFAR-10. TS does not change the base model CW-ECE much; in some cases there is no change and the orange and blue lines intersect. In all cases, non-normalized HB reduces the CW-ECE significantly, and normalization hurts HB significantly.

Theorem 2. Fix hyperparameters $\delta > 0$ (arbitrarily small) and points per bin $k_1, k_2, \dots, k_l \geq 2$, and assume $n_l \geq k_l$ for every $l \in [L]$. Then, for every $l \in [L]$, for any $\alpha_l \in (0, 1)$, Algorithm 2 is $(\epsilon^{(1)}, \alpha)$ -marginally and $(\epsilon^{(2)}, \alpha)$ -conditionally class-wise calibrated with

$$\epsilon_l^{(1)} = \sqrt{\frac{\log(2/\alpha_l)}{2(k_l - 1)}} + \delta, \quad \text{and} \quad \epsilon_l^{(2)} = \sqrt{\frac{\log(2n/k_l\alpha_l)}{2(k_l - 1)}} + \delta. \quad (12)$$

Further, for any distribution P over $\mathcal{X} \times [L]$,

- (a) $P(\text{CW-ECE}(c, h) \leq \max_{l \in [L]} \epsilon_l^{(2)}) \geq 1 - \sum_{l \in [L]} \alpha_l$, and
- (b) $\mathbb{E}[\text{CW-ECE}(c, h)] \leq \max_{l \in [L]} \sqrt{1/2k_l} + \delta$.

Theorem 2 is proved in Appendix C. The proof follows by using the result of Gupta and Ramdas [2021, Theorem 2], derived in the binary calibration setting, for each h_l separately.

As discussed in Section 3, unlike previous works [Guo et al., 2017, Kull et al., 2019, Zadrozny and Elkan, 2002], Algorithm 2 does not normalize the h_l 's. We do not know how to derive Theorem 2 style results for a normalized version of Algorithm 2.

Figure 6 presents estimated CW-ECE values for four deep net architectures trained using two loss functions on CIFAR-10 across different values for the numbers of bins, and Figure 7 presents the same results on CIFAR-100. These plots compare the base model, temperature scaling, non-normalized HB and normalized HB, same as the plots in Figure 5 of the main paper; the plots from the main paper are also reproduced to ease comparison. In both plots, we find that non-normalized HB performs much better than both the base model and temperature scaling, across all deep net architectures that we considered.

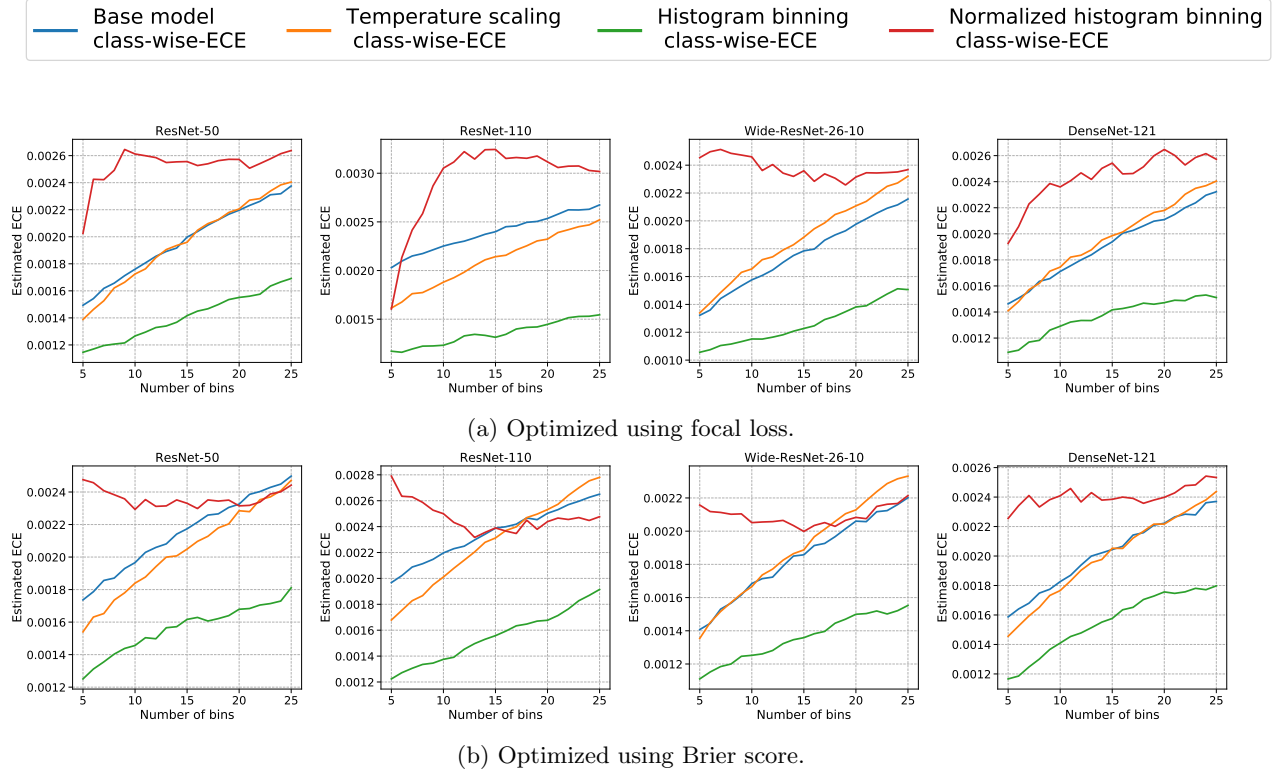


Figure 7: CW-ECE of histogram binning (HB) and temperature scaling (TS) with deep nets on CIFAR-100. TS does not change the base model CW-ECE much; HB reduces it significantly, and normalization hurts HB significantly.

In some plots, such as the Wide-Resnet-26-10 plot in Figure 5b and Figure 6b, the blue base model line and the orange temperature scaling line intersect. This is not surprising; it occurs since the optimal temperature on the calibration data was learnt to be $T = 1$, which corresponds to not changing the base model at all. Even in such cases when temperature scaling changes the base model by a little, or not at all, top-label HB shows improved performance.

B Binning schemes for canonical multiclass calibration

Let $\mathbf{g} : \mathcal{X} \rightarrow \Delta^{L-1}$ be a base model. The goal in post-hoc canonical calibration is to use the calibration data \mathcal{D} and \mathbf{g} to learn an approximately calibrated $\mathbf{h} : \mathcal{X} \rightarrow \Delta^{L-1}$. The basic framework for achieving approximate canonical calibration using binning relies on a binning scheme, which is a partitioning of Δ^{L-1} into $B \geq 1$ bins. We denote this binning scheme as $\mathcal{B} : \Delta^{L-1} \rightarrow [B]$, where $\mathcal{B}(\mathbf{s})$ corresponds to the bin to which $\mathbf{s} \in \Delta^{L-1}$ belongs. To learn \mathbf{h} , the calibration data is binned to get sets of data-point indices that belong to each bin, depending on the $\mathbf{g}(X_i)$ values:

$$\text{for every } b \in [B], T_b := \{i : \mathcal{B}(\mathbf{g}(X_i)) = b\}, n_b = |T_b|.$$

We then compute the following estimates for the label probabilities in each bin:

$$\text{for every } (l, b) \in [L] \times [B], \hat{\Pi}_{l,b} := \frac{\sum_{i \in T_b} \mathbb{1}\{Y_i = l\}}{n_b} \text{ if } n_b > 0 \text{ else } \hat{\Pi}_{l,b} = 1/B.$$

The binning predictor $\mathbf{h} : \mathcal{X} \rightarrow \Delta^{L-1}$ is now defined component-wise as follows:

$$\text{for every } l \in [L], h_l(x) = \hat{\Pi}_{l, \mathcal{B}(x)}.$$

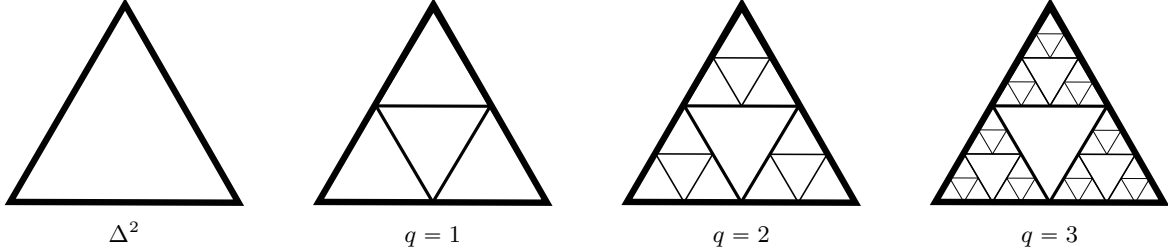


Figure 8: Sierpinski binning for $L = 3$. The leftmost triangle represents the probability simplex Δ^2 . Sierpinski binning divides Δ^2 recursively based on a depth parameter $q \in \mathbb{N}$.

In words, for every bin $b \in [B]$, \mathbf{h} predicts the empirical distribution of the Y values in bin b .

Using a multinomial concentration inequality [Devroye, 1983, Qian et al., 2020, Weissman et al., 2003], calibration guarantees can be shown for the learnt \mathbf{h} . Podkopaev and Ramdas [2021, Theorem 3] show such a result using the Bretagnolle-Huber-Carol inequality. All of these concentration inequality give bounds that depend inversely on n_b or $\sqrt{n_b}$.

In the following subsections, we describe some binning schemes which can be used for canonical calibration based on the setup illustrated above. First we describe fixed schemes that are not adaptive to the distribution of the data: Sierpinski binning (Appendix B.1) and grid-style binning (Appendix B.2). These are analogous to fixed-width binning for $L = 2$. Fixed binning schemes are not adapted to the calibration data and may have highly imbalanced bins leading to poor estimation of the distribution of \mathbf{Y} in bins with small n_b . In the binary case, this issue is remedied using histogram binning to ensure that each bin has nearly the same number of calibration points [Gupta and Ramdas, 2021]. While histogram binning uses the order of the scalar $g(X_i)$ values, there is no obvious ordering for the multi-dimensional $\mathbf{g}(X_i)$ values. In Appendix B.3 we describe a projection based histogram binning scheme that circumvents this issue and ensures that each n_b is reasonably large. In Appendix B.4, we present some preliminary experimental results using our proposed binning schemes.

Certain asymptotic consistency results different from calibration have been established for histogram regression and classification in the nonparametric statistics literature [Breiman et al., 2017, Devroye, 1988, Gordon and Olshen, 1984, Lugosi and Nobel, 1996, Nobel, 1996]; further extensive references can be found within these works. The methodology of histogram regression and classification relies on binning and is very similar to the one we propose here. The main difference is that these works consider binning the feature space \mathcal{X} directly, unlike the post-hoc setting where we are essentially interested in binning Δ^{L-1} . In terms of theory, the results these works target are asymptotic consistency for the (Bayes) optimal classification and regression functions, instead of canonical calibration. It would be interesting to consider the (finite-sample) canonical calibration properties of the various algorithms proposed in the context of histogram classification. However, such a study is beyond the scope of this paper.

B.1 Sierpinski binning

First, we describe Sierpinski binning for $L = 3$. The probability simplex for $L = 3$, Δ^2 , is a triangle with vertices $\mathbf{e}_1 = (1, 0, 0)$, $\mathbf{e}_2 = (0, 1, 0)$, and $\mathbf{e}_3 = (0, 0, 1)$. Sierpinski binning is a recursive partitioning of this triangle based on the fractal popularly known as the Sierpinski triangles. Some Sierpinski bins for $L = 3$ are shown in Figure 8. Formally, we define Sierpinski binning recursively based on a depth parameter $q \in \mathbb{N}$. Given an $x \in \mathcal{X}$, let $\mathbf{s} = \mathbf{g}(x)$. For $q = 1$, the number of bins is $B = 4$, and the binning scheme \mathcal{B} is defined as:

$$\mathcal{B}(\mathbf{s}) = \begin{cases} 1 & \text{if } s_1 > 0.5 \\ 2 & \text{if } s_2 > 0.5 \\ 3 & \text{if } s_3 > 0.5 \\ 4 & \text{otherwise.} \end{cases} \quad (13)$$

Note that since $s_1 + s_2 + s_3 = 1$, only one of the above conditions can be true. It can be verified that each of the bins have volume equal to $(1/4)$ -th the volume of the probability simplex Δ^2 . If a finer resolution of Δ^2

is desired, B can be increased by further dividing the partitions above. Note that each partition is itself a triangle; thus each triangle can be mapped to Δ^2 to recursively define the sub-partitioning. For $i \in [4]$, define the bins $b_i = \{\mathbf{s} : \mathcal{B}(\mathbf{s}) = i\}$. Consider the bin b_1 . Let us ‘reparameterize’ it as $(t_1, t_2, t_3) = (2s_1 - 1, 2s_2, 2s_3)$. It can be verified that

$$b_1 = \{(t_1, t_2, t_3) : s_1 > 0.5\} = \{(t_1, t_2, t_3) : t_1 + t_2 + t_3 = 1, t_1 \in (0, 1], t_2 \in [0, 1), t_3 \in [0, 1)\}.$$

Based on this reparameterization, we can recursively sub-partition b_1 as per the scheme (13), replacing s with t . Such reparameterizations can be defined for each of the bins defined in (13):

$$\begin{aligned} b_2 &= \{(s_1, s_2, s_3) : s_2 > 0.5\} : (t_1, t_2, t_3) = (2s_1, 2s_2 - 1, 2s_3), \\ b_3 &= \{(s_1, s_2, s_3) : s_3 > 0.5\} : (t_1, t_2, t_3) = (2s_1, 2s_2, 2s_3 - 1), \\ b_4 &= \{(s_1, s_2, s_3) : s_i \leq 0.5 \text{ for all } i\} : (t_1, t_2, t_3) = (1 - 2s_1, 1 - 2s_2, 1 - 2s_3), \end{aligned}$$

and thus every bin can be recursively sub-partitioned as per (13). As illustrated in Figure 8, for Sierpinski binning, we sub-partition only the bins b_1, b_2, b_3 since the bin b_4 corresponds to low confidence for all labels, where finer calibration may not be needed. (Also, in the $L > 3$ case described shortly, the corresponding version of b_4 is geometrically different from Δ^{L-1} , and the recursive partitioning cannot be defined for it.) If at every depth, we sub-partition all bins except the corresponding b_4 bins, then it can be shown using simple algebra that the total number of bins is $(3^{q+1} - 1)/2$. For example, in Figure 8, when $q = 2$, the number of bins is $B = 14$, and when $q = 3$, the number of bins is $B = 40$.

As in the case of $L = 3$, Sierpinski binning for general L is defined through a partitioning function of Δ^{L-1} into $L + 1$ bins, and a reparameterization of the partitions so that they can be further sub-partitioned. The $L + 1$ bins at depth $q = 1$ are defined as

$$\mathcal{B}(\mathbf{s}) = \begin{cases} l & \text{if } s_l > 0.5, \\ L + 1 & \text{otherwise.} \end{cases} \quad (14)$$

While this looks similar to the partitioning (13), the main difference is that the bin b_{L+1} has a larger volume than other bins. Indeed for $l \in [L]$, $\text{vol}(b_l) = \text{vol}(\Delta^{L-1})/2^{L-1}$, while $\text{vol}(b_{L+1}) = \text{vol}(\Delta^{L-1})(1 - L/2^{L-1}) \geq \text{vol}(\Delta^{L-1})/2^{L-1}$, with equality only occurring for $L = 3$. Thus the bin b_{L+1} is larger than the other bins. If $\mathbf{g}(x) \in b_{L+1}$, then the prediction for x may be not be very sharp, compared to if $\mathbf{g}(x)$ were in any of the other bins. On the other hand, if $\mathbf{g}(x) \in b_{L+1}$, the score for every class is smaller than 0.5, and sharp calibration may often not be desired in this region.

In keeping with this understanding, we only reparameterize the bins b_1, b_2, \dots, b_L so that they can be further divided:

$$b_l = \{(s_1, s_2, \dots, s_L) : s_l > 0.5\} : (t_1, t_2, \dots, t_L) = (2s_1, \dots, 2s_l - 1, \dots, 2s_L).$$

For every $l \in [L]$, under the reparameterization above, it is straightforward to verify that

$$\{(t_1, t_2, \dots, t_L) : s_l > 0.5\} = \{(t_1, t_2, \dots, t_L) : \sum_{u \in [L]} t_u = 1, t_l \in (0, 1], t_u \in [0, 1) \forall u \neq l\}.$$

Thus every bin can be recursively sub-partitioned following (14). For Sierpinski binning with L labels, the number of bins at depth q is given by $(L^{q+1} - 1)/(L - 1)$.

B.2 Grid-style binning

Grid-style binning is motivated from the 2D reliability diagrams of Widmann et al. [2019, Figure 1], where they partitioned Δ^2 into multiple equi-volume bins in order to assess canonical calibration on a 3-class version of CIFAR-10. For $L = 3$, Δ^2 can be divided as shown in Figure 9. This corresponds to ‘gridding’ the space Δ^2 , just the way we think of ‘gridding’ the real hyperplane. However, the mathematical description of this grid for general L is not apparent from Figure 9. We describe grid-style binning formally for general $L \geq 3$.

Consider some $\tau > 0$ such that $K := 1/\tau \in \mathbb{N}$. For every tuple $\mathbf{k} = (k_1, k_2, \dots, k_L)$ in the set

$$I = \{\mathbf{k} \in \mathbb{N}^L : \max(L, K + 1) \leq \sum_{l \in [L]} k_l \leq K + (L - 1)\}, \quad (15)$$

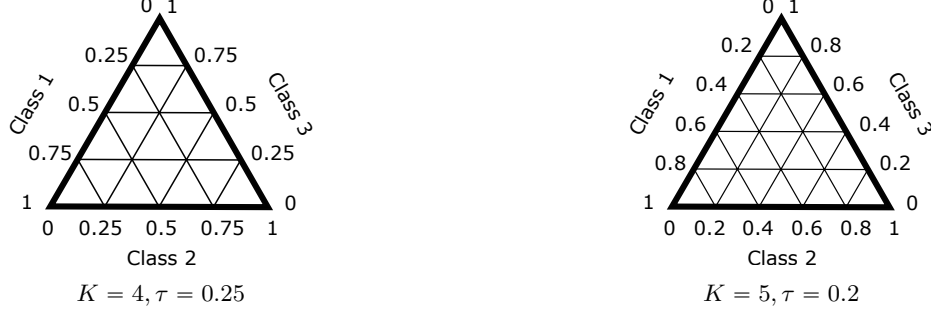


Figure 9: Grid-style binning for $L = 3$.

define the bins

$$b_{\mathbf{k}} := \{\mathbf{s} \in \Delta^{L-1} : \text{for every } l \in [L], s_l K \in [k_l - 1, k_l]\}. \quad (16)$$

These bins are not mutually disjoint, but intersections can only occur at the ‘edges’. That is, for every \mathbf{s} that belongs to more than one bin, at least one component s_l satisfies $s_l K \in \mathbb{N}$. In order to identify a single bin \mathbf{s} , ties can be broken arbitrarily. One strategy is to use some ordering on \mathbb{N}^L ; say for $\mathbf{k}_1 \neq \mathbf{k}_2 \in \mathbb{N}$, $\mathbf{k}_1 < \mathbf{k}_2$ if and only if for the first element of \mathbf{k}_1 that is unequal to the corresponding element of \mathbf{k}_2 the one corresponding to \mathbf{k}_1 is smaller. Then define the binning function $\mathcal{B} : \Delta^{L-1} \rightarrow |I|$ as $\mathcal{B}(\mathbf{s}) = \min\{\mathbf{k} : \mathbf{s} \in b_{\mathbf{k}}\}$. The following propositions prove that a) each \mathbf{s} belongs to at least one bin, and b) that every bin is an $L-1$ dimensional object (and thus a meaningful partition of Δ^{L-1}).

Proposition 3. *The bins $\{b_{\mathbf{k}} : \mathbf{k} \in I\}$ defined by (16) mutually exhaust Δ^{L-1} .*

Proof. Consider any $\mathbf{s} \in \Delta^{L-1}$. For $s_l K \notin \mathbb{N} = \{1, 2, \dots\}$, set $k_l = \max(1, \lceil s_l K \rceil) > s_l K$. Consider the condition

$$C : \text{for all } l \text{ such that } s_l K \notin \mathbb{N}, s_l K = 0.$$

If C is true, then for l such that $s_l K \in \mathbb{N}$, set $k_l = s_l K$. If C is not true, then for l such that $s_l K \in \mathbb{N}$, set exactly one $k_l = s_l K + 1$, and for the rest set $k_l = s_l K$. Based on this setting of \mathbf{k} , it can be verified that $\mathbf{s} \in b_{\mathbf{k}}$.

Further, note that for every l , $k_l \geq s_l K$, and there exists at least one l such that $k_l > s_l K$. Thus we have:

$$\begin{aligned} \sum_{l=1}^L k_l &> \sum_{l=1}^L s_l K \\ &= K. \end{aligned}$$

Since $\sum_{l=1}^L k_l \in \mathbb{N}$, we must have $\sum_{l=1}^L k_l \geq K + 1$. Further since each $k_l \in \mathbb{N}$, $\sum_{l=1}^L k_l \geq L$.

Next, note that for every l , $k_l \leq s_l K + 1$. If C is true, then there is at least one l such that $s_l K \in \mathbb{N}$, and for this l , we have set $k_l = s_l K < s_l K + 1$. If C is not true, then either there exists at least one l such that $s_l K \notin \mathbb{N} \cup \{0\}$ for which $k_l = \lceil s_l K \rceil < s_l K + 1$, or every $s_l K \in \mathbb{N}$, in which case we have set $k_l = s_l K$ for one of them. In all cases, note that there exists an l such that $k_l < s_l K + 1$. Thus,

$$\begin{aligned} \sum_{l=1}^L k_l &< \sum_{l=1}^L (s_l K + 1) \\ &= K + L. \end{aligned}$$

Since $\sum_{l=1}^L k_l \in \mathbb{N}$, we must have $\sum_{l=1}^L k_l \leq K + L - 1$. □

Next, we show that each bin indexed by $\mathbf{k} \in I$ contains a non-zero volume subset of Δ^{L-1} , where volume is defined with respect to the Lebesgue measure in \mathbb{R}^{L-1} . This can be shown by arguing that $b_{\mathbf{k}}$ contains a scaled and translated version of Δ^{L-1} .

Algorithm 3: Projection histogram binning for canonical calibration

Input: Base multiclass predictor $\mathbf{g} : \mathcal{X} \rightarrow \Delta^{L-1}$, calibration data
 $\mathcal{D} = \{(X_1, Y_1), (X_2, Y_2), \dots, (X_n, Y_n)\}$

Hyperparameter: number of bins B , unit vectors $q_1, q_2, \dots, q_B \in \mathbb{R}^L$,

Output: Approximately calibrated scoring function \mathbf{h}

- 1 $S \leftarrow \{\mathbf{g}(X_1), \mathbf{g}(X_2), \dots, \mathbf{g}(X_n)\};$
- 2 $T \leftarrow$ empty array of size B ;
- 3 $c \leftarrow \lfloor \frac{n+1}{B} \rfloor$;
- 4 **for** $b \leftarrow 1$ **to** $B - 1$ **do**
- 5 $T_b \leftarrow$ order-statistics(S, q_b, c);
- 6 $S \leftarrow S \setminus \{v \in S : v^T q_b \leq T_b\}$;
- 7 **end**
- 8 $T_B \leftarrow 1.01$;
- 9 $\mathcal{B}(\mathbf{g}(\cdot)) \leftarrow \min\{b \in [B] : \mathbf{g}(\cdot)^T q_b < T_b\}$;
- 10 $\hat{\Pi} \leftarrow$ empty matrix of size $B \times L$;
- 11 **for** $b \leftarrow 1$ **to** B **do**
- 12 **for** $l \leftarrow 1$ **to** L **do**
- 13 $\hat{\Pi}_{b,l} \leftarrow \text{Mean}\{\mathbb{1}\{Y_i = l\} : \mathcal{B}(\mathbf{g}(X_i)) = b \text{ and } \forall s \in [B], \mathbf{g}(X_i)^T q_s \neq T_s\}$;
- 14 **end**
- 15 **end**
- 16 **for** $l \leftarrow 1$ **to** L **do**
- 17 $h_l(\cdot) \leftarrow \hat{\Pi}_{\mathcal{B}(\mathbf{g}(\cdot)), l}$;
- 18 **end**
- 19 **return** \mathbf{h} ;

Proposition 4. For every $\mathbf{k} \in I$, there exists some $\mathbf{u} \in \mathbb{R}^L$ and $v > 0$ such that $\mathbf{u} + v\Delta^{L-1} \subseteq b_{\mathbf{k}}$.

Proof. Fix some $\mathbf{k} \in I$. By condition (15), $\sum_{l=1}^L k_l \in [\max(L, K + 1), K + L - 1]$. Based on this, we claim that there exists a $\tau \in [0, 1)$ such that

$$\sum_{l=1}^L (k_l - 1) + \tau L + (1 - \tau) = K. \quad (17)$$

Indeed, note that for $\tau = 0$, $\sum_{l=1}^L (k_l - 1) + \tau L + (1 - \tau) \leq (K - 1) + 1 = K$ and for $\tau = 1$, $\sum_{l=1}^L (k_l - 1) + \tau L + (1 - \tau) = \sum_{l=1}^L k_l > K$. Thus, there exists a τ that satisfies (17) by the intermediate value theorem.

Next, define $\mathbf{u} = K^{-1}(\mathbf{k} + (\tau - 1)\mathbf{1}_L)$ and $v = K^{-1}(1 - \tau) > 0$, where $\mathbf{1}_L$ denotes the vector in \mathbb{R}^L with each component equal to 1. Consider any $\mathbf{s} \in \mathbf{u} + v\Delta^{L-1}$. Note that for every $l \in [L]$, $s_l K \in [k_l - 1, k_l]$ and by property (17),

$$\sum_{l=1}^L s_l K = \left(\sum_{l=1}^L (k_l + (\tau - 1)) \right) + v = \sum_{l=1}^L (k_l - 1) + \tau L + (1 - \tau) = K.$$

Thus, $\mathbf{s} \in \Delta^{L-1}$ and by the definition of $b_{\mathbf{k}}$, $\mathbf{s} \in b_{\mathbf{k}}$. This completes the proof. \square

The previous two propositions imply that \mathcal{B} satisfies the property we require of a reasonable binning scheme. For $L = 3$, grid-style binning gives equi-volume bins as illustrated in Figure 9; however this is not true for $L > 3$. We now describe a histogram binning based partitioning scheme.

B.3 Projection based histogram binning for canonical calibration

Some of the bins defined by Sierpinski binning and grid-style binning may have very few calibration points n_b , leading to poor estimation of $\hat{\Pi}$. In the binary calibration case, this can be remedied using histogram

binning which strongly relies on the scoring function g taking values in a fully ordered space $[0, 1]$. To ensure that each bin contains $\Omega(n/B)$ points, we estimate the quantiles of $g(X)$ and created the bins as per these quantiles. However, there are no natural quantiles for unordered prediction spaces such as Δ^{L-1} ($L \geq 3$). In this section, we develop a histogram binning scheme for Δ^{L-1} that is semantically interpretable and has desirable statistical properties.

Our algorithm takes as input a prescribed number of bins B and an arbitrary sequence of vectors $q_1, q_2, \dots, q_{B-1} \in \mathbb{R}^L$ with unit ℓ_2 -norm: $\|q_i\|_2 = 1$. Each of these vectors represents a direction on which we will project Δ^{L-1} in order to induce a full order on Δ^{L-1} . Then, for each direction, we will use an order statistics on the induced full order to identify a bin with exactly $\lfloor (n+1)/B \rfloor - 1$ calibration points (except the last bin, which may have more points). The formal algorithm is described in Algorithm 3. It uses the following new notation: given m vectors $v_1, v_2, \dots, v_m \in \mathbb{R}^L$, a unit vector u , and an index $j \in [m]$, let order-statistics($\{v_1, v_2, \dots, v_m\}, u, j$) denote the j -th order-statistics of $\{v_1^T u, v_2^T u, \dots, v_m^T u\}$.

We now briefly describe some values computed by Algorithm 3 in words to build intuition. The array T , which is learnt on the data, represents the identified thresholds for the directions given by q . Each (q_b, T_b) pair corresponds to a hyperplane that ‘cuts’ Δ^{L-1} into two subsets given by $\{x \in \Delta^{L-1} : x^T q_b < T_b\}$ and $\{x \in \Delta^{L-1} : x^T q_b \geq T_b\}$. The overall partitioning of Δ^{L-1} is created by merging these cuts sequentially. This defines the binning function \mathcal{B} . By construction, the binning function is such that each bin contains at least $\lfloor \frac{n+1}{B} \rfloor - 1$ many points in its interior. As suggested by Gupta and Ramdas [2021], we do not include the points that lie on the boundary, that is, points X_i that satisfy $\mathbf{g}(X_i)^T q_s = T_s$ for some $s \in [B]$. The interior points bins are then used to estimate the bin biases $\hat{\Pi}$.

No matter how the q -vectors are chosen, the bins created by Algorithm 3 have at least $\lfloor \frac{n}{B} \rfloor - 1$ points for bias estimation. However, we discuss some simple heuristics for setting q that are semantically meaningful. For some intuition, note that the binary version of histogram binning Gupta and Ramdas [2021, Algorithm 1] is essentially recovered by Algorithm 3 if $L = 2$ by setting each q_b as \mathbf{e}_2 (the vector $[0, 1]$). Equivalently, we can set each q_b to $-\mathbf{e}_1$ since both are equivalent for creating a projection-based order on Δ_2 . Thus for $L \geq 3$, a natural strategy for the q -vectors is to rotate between the canonical basis vectors: $q_1 = -\mathbf{e}_1, q_2 = -\mathbf{e}_2, \dots, q_L = -\mathbf{e}_L, q_{L+1} = -\mathbf{e}_1, \dots$, and so on. Projecting with respect to $-\mathbf{e}_l$ focuses on the class l by forming a bin corresponding to the largest values of $g_l(X_i)$ among the remaining X_i ’s which have not yet been binned. (On the other hand, projecting with respect to \mathbf{e}_l will correspond to forming a bin with the smallest values of $g_l(X_i)$.)

The q -vectors can also be set adaptively based on the training data (without seeing the calibration data). For instance, if most points belong to a specific class $l \in [L]$, we may want more sharpness for this particular class. In that case, we can choose a higher ratio of the q -vectors to be $-\mathbf{e}_l$.

B.4 Experiments with the COVTYPE dataset

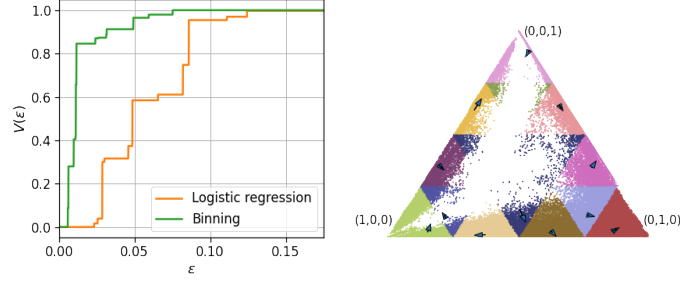
In Figure 10 we illustrate the binning schemes proposed in this section on a 3-class version of the COVTYPE-7 dataset considered in Section 2.2. As noted before, this is an imbalanced dataset where classes 1 and 2 dominate. We created a 3 class problem with the classes 1, 2, and other (as class 3). The entire dataset has 581012 points and the ratio of the classes is approximately 36%, 49%, 15% respectively. The dataset was split into train-test in the ratio 70:30. The training data was further split into modeling-calibration in the ratio 90:10. A logistic regression model \mathbf{g} using `sklearn.linear_model.LogisticRegression` was learnt on the modeling data, and \mathbf{g} was recalibrated on the calibration data.

The plots on the right in Figure 10 are *recalibration diagrams*. The base predictions $\mathbf{g}(X)$ on the test-data are displayed as a scatter plot on Δ^2 . Points in different bins are colored using one of 10 different colors (since the number of bins is larger than 10, some colors correspond to more than one bin). For each bin, an arrow is drawn, where the tail of the arrow corresponds to the average $\mathbf{g}(X)$ predictions in the bin and the head of the arrow corresponds to the recalibrated $\mathbf{h}(X)$ prediction for the bin. For bins that contained very few points, the arrows are suppressed for visual clarity.

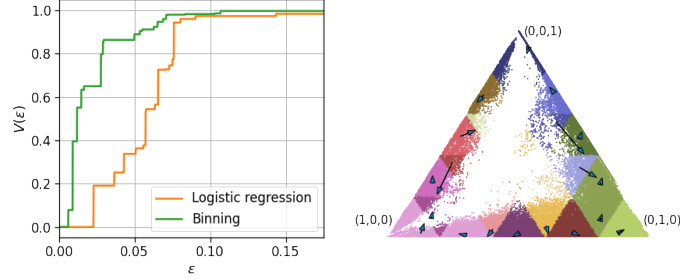
The plots on the left in Figure 10 are validity plots [Gupta and Ramdas, 2021]. Validity plots display estimates of

$$V(\varepsilon) = P_{\text{test-data}} (\|\mathbb{E}[\mathbf{Y} | \mathbf{g}(X)] - \mathbf{g}(X)\|_1 \leq \varepsilon),$$

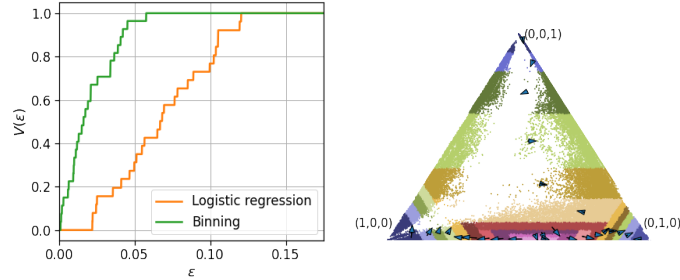
as ε varies (\mathbf{g} corresponds to the validity plot for logistic regression; replacing \mathbf{g} with \mathbf{h} above gives plots for



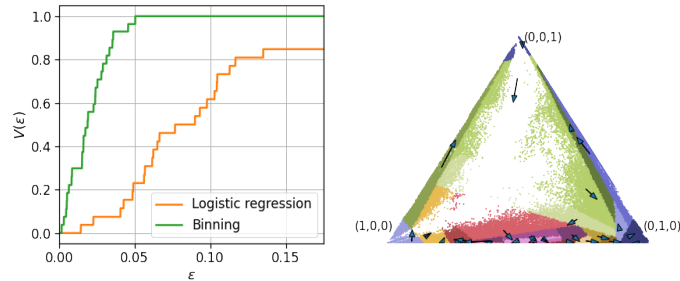
(a) Calibration using Sierpinski binning at depth $q = 2$.



(b) Calibration using grid-style binning with $K = 5$, $\tau = 0.2$.



(c) Projection-based HB with $B = 27$ projections: $q_1 = -\mathbf{e}_1, q_2 = -\mathbf{e}_2, \dots, q_4, -\mathbf{e}_1, \dots$, and so on.



(d) Projection-based HB with $B = 27$ random projections (q_i drawn uniformly from the ℓ_2 -unit-ball in \mathbb{R}^3).

Figure 10: Canonical calibration using fixed and histogram binning on a 3-class version of the COVTYPE-7 dataset. The reliability diagrams (left) indicate that all forms of binning improve the calibration of the base logistic regression model. The recalibration diagrams (right) are a scatter plot of the predictions $\mathbf{g}(X)$ on the test data with the points colored in 10 different colors depending on their bin. For every bin, the arrow-tail indicates the mean probability predicted by the base model \mathbf{g} whereas the arrow-head indicates the probability predicted by the updated model \mathbf{h} .

the binning based classifier \mathbf{h}). For logistic regression, the same binning scheme as the one provided by \mathbf{h} is used to estimate $V(\varepsilon)$.

Overall, Figure 10 shows that all of the binning approaches improve the calibration of the original logistic regression model across different ε . However, the recalibration does not change the original model significantly. Comparing the different binning methods to each other, we find that they all perform quite similarly. It would be interesting to further study these and other binning methods for post-hoc canonical calibration.

C Proofs

Proofs appear in separate subsections, in the same order as the corresponding results appear in the paper.

C.1 Proof of Proposition 1

To avoid confusion between the the conditioning operator and the absolute value operator $|\cdot|$, we use $\text{abs}(\cdot)$ to denote absolute values below. Note that,

$$\begin{aligned} \text{abs}(P(Y = c(X) | h(X)) - h(X)) &= \text{abs}(\mathbb{E}[\mathbb{1}\{Y = c(X)\} | h(X)] - h(X)) \\ &= \text{abs}(\mathbb{E}[\mathbb{1}\{Y = c(X)\} - h(X) | h(X)]) \\ &= \text{abs}(\mathbb{E}[\mathbb{E}[\mathbb{1}\{Y = c(X)\} - h(X) | h(X), c(X)] | h(X)]) \\ &\leq \mathbb{E}[\text{abs}(\mathbb{E}[\mathbb{1}\{Y = c(X)\} - h(X) | h(X), c(X)]) | h(X)] \\ &\quad \text{(by Jensen's inequality)} \\ &= \mathbb{E}[\text{abs}(P(Y = c(X) | h(X), c(X)) - h(X)) | h(X)]. \end{aligned}$$

Thus,

$$\begin{aligned} \text{conf-ECE}(c, h) &= \mathbb{E}[\text{abs}(P(Y = c(X) | h(X)) - h(X))] \\ &\leq \mathbb{E}[\mathbb{E}[\text{abs}(P(Y = c(X) | h(X), c(X)) - h(X)) | h(X)]] \\ &= \mathbb{E}[\text{abs}(P(Y = c(X) | h(X), c(X)) - h(X))] \\ &= \text{TL-ECE}(c, h). \end{aligned}$$

□

C.2 Proof of Theorem 1

The proof strategy is as follows. First, we use the bound of Gupta and Ramdas [2021, Theorem 4] (henceforth called the GR21 bound), derived in the binary calibration setting, to conclude marginal, conditional, and ECE guarantees for each h_l . Then, we show that the binary guarantees for the individual h_l 's leads to a top-label guarantee for the overall predictor (c, h) .

Consider any $l \in [L]$. Let P_l denote the conditional distribution of $(X, \mathbb{1}\{Y = l\})$ given $c(X) = l$. Clearly, D_l is a set of n_l i.i.d. samples from P_l , and h_l is learning a binary calibrator with respect to P_l using binary histogram binning. The number of data-points is n_l and the number of bins is $B_l = \lfloor n_l/k \rfloor$ bins. We now apply the GR21 bounds on h_l . First, we verify that the condition they require is satisfied:

$$n_l \geq k \lfloor n_l/k \rfloor \geq 2B_l.$$

Thus their marginal calibration bound for h_l gives,

$$P\left(|P(Y = l | c(X) = l, h_l(X)) - h_l(X)| \leq \delta + \sqrt{\frac{\log(2/\alpha)}{2(\lfloor n_l/B_l \rfloor - 1)}} \mid c(X) = l\right) \geq 1 - \alpha.$$

Note that since $\lfloor n_l/B_l \rfloor = \lfloor n_l/\lfloor n_l/k \rfloor \rfloor \geq k$,

$$\varepsilon_1 = \delta + \sqrt{\frac{\log(2/\alpha)}{2(k-1)}} \geq \delta + \sqrt{\frac{\log(2/\alpha)}{2(\lfloor n_l/B_l \rfloor - 1)}}.$$

Thus we have

$$P(|P(Y = l | c(X) = l, h_l(X)) - h_l(X)| \leq \varepsilon_1 | c(X) = l) \geq 1 - \alpha.$$

This is satisfied for every l . Using the law of total probability gives us the top-label marginal calibration guarantee for (c, h) :

$$\begin{aligned} & P(|P(Y = c(X) | c(X), h(X)) - h(X)| \leq \varepsilon_1) \\ &= \sum_{l=1}^L P(c(X) = l) P(|P(Y = c(X) | c(X), h(X)) - h(X)| \leq \varepsilon_1 | c(X) = l) \\ & \quad \text{(law of total probability)} \\ &= \sum_{l=1}^L P(c(X) = l) P(|P(Y = l | c(X) = l, h_l(X)) - h_l(X)| \leq \varepsilon_1 | c(X) = l) \\ & \quad \text{(by construction, if } c(x) = l, h(x) = h_l(x)) \\ &\geq \sum_{l=1}^L P(c(X) = l)(1 - \alpha) \\ &= 1 - \alpha. \end{aligned}$$

Similarly, the in-expectation ECE bound of GR21, for $p = 1$, gives for every l ,

$$\begin{aligned} \mathbb{E}|P(Y = l | c(X) = l, h_l(X)) - h_l(X) | c(X) = l| &\leq \sqrt{B_l/2n_l} + \delta \\ &= \sqrt{\lfloor n_l/k \rfloor / 2n_l} + \delta \\ &\leq \sqrt{1/2k} + \delta. \end{aligned}$$

Thus,

$$\begin{aligned} & \mathbb{E}|P(Y = c(X) | c(X), h_l(X)) - h(X)| \\ &= \sum_{l=1}^L P(c(X) = l) \mathbb{E}|P(Y = l | c(X) = l, h_l(X)) - h_l(X)| | c(X) = l \\ &\leq \sum_{l=1}^L P(c(X) = l)(\sqrt{1/2k} + \delta) \\ &= \sqrt{1/2k} + \delta. \end{aligned}$$

Next, we show the top-label conditional calibration bound. Let $B = \sum_{l=1}^L B_l$ and $\alpha_l = \alpha B_l/B$. Note that $B \leq \sum_{l=1}^L n_l/k = n/k$. The binary conditional calibration bound of GR21 gives

$$P\left(\forall r \in \text{Range}(h_l), |P(Y = l | c(X) = l, h_l(X) = r) - r| \leq \delta + \sqrt{\frac{\log(2B_l/\alpha_l)}{2(\lfloor n_l/B_l \rfloor - 1)}} | c(X) = l\right) \geq 1 - \alpha_l.$$

Note that

$$\sqrt{\frac{\log(2B_l/\alpha_l)}{2(\lfloor n_l/B_l \rfloor - 1)}} = \sqrt{\frac{\log(2B/\alpha)}{2(\lfloor n_l/B_l \rfloor - 1)}}$$

$$\begin{aligned}
&\leq \sqrt{\frac{\log(2n/k\alpha)}{2(\lfloor n_l/B_l \rfloor - 1)}} && \text{(since } B \leq n/k) \\
&\leq \sqrt{\frac{\log(2n/k\alpha)}{2(k-1)}} && \text{(since } k \leq \lfloor n_l/B_l \rfloor).
\end{aligned}$$

Thus for every $l \in [L]$,

$$P(\forall r \in \text{Range}(h_l), |P(Y = l \mid c(X) = l, h_l(X) = r) - r| \leq \varepsilon_2) \geq 1 - \alpha_l.$$

By construction of h , conditioning on $c(X) = l$ and $h_l(X) = r$ is the same as conditioning on $c(X) = l$ and $h(X) = r$. Taking a union bound over all L gives

$$\begin{aligned}
P(\forall l \in [L], r \in \text{Range}(h), |P(Y = c(X) \mid c(X) = l, h(X) = r) - r| \leq \varepsilon_2) \\
\geq 1 - \sum_{l=1}^L \alpha_l = 1 - \alpha,
\end{aligned}$$

proving the conditional calibration result. Finally, note that if for every $l \in [L], r \in \text{Range}(h)$,

$$|P(Y = c(X) \mid c(X) = l, h(X) = r) - r| \leq \varepsilon_2,$$

then also

$$\text{TL-ECE}(c, h) = \mathbb{E}|P(Y = c(X) \mid h(X), c(X)) - h(X)| \leq \varepsilon_2.$$

This proves the high-probability bound for the TL-ECE. \square

Remark 1. Gupta and Ramdas [2021] proved a more general result for general ℓ_p -ECE bounds. Similar results can also be derived for the suitably defined ℓ_p -TL-ECE. Additionally, it can be shown that with probability $1 - \alpha$, the TL-MCE of (c, h) is bounded by ε_2 . (TL-MCE is defined in Appendix D.2, equation (20).)

C.3 Proof of Proposition 2

Consider a specific $l \in [L]$. We use h_l to denote the l 'th component function of \mathbf{h} and $Y_l = \mathbb{1}\{Y = l\}$. Canonical calibration implies

$$P(Y = l \mid \mathbf{h}(X)) = \mathbb{E}[Y_l \mid \mathbf{h}(X)] = h_l(X). \quad (18)$$

We can then use the law of iterated expectations (or tower rule) to get the final result:

$$\begin{aligned}
\mathbb{E}[Y_l \mid h_l(X)] &= \mathbb{E}[\mathbb{E}[Y_l \mid \mathbf{h}(X)] \mid h_l(X)] \\
&= \mathbb{E}[h_l(X) \mid h_l(X)] && \text{(by the canonical calibration property (18))} \\
&= h_l(X).
\end{aligned}$$

\square

C.4 Proof of Theorem 2

We use the bounds of Gupta and Ramdas [2021, Theorem 4] (henceforth called the GR21 bounds), derived in the binary calibration setting, to conclude marginal, conditional, and ECE guarantees for each h_l . This leads to the class-wise results as well.

Consider any $l \in [L]$. Let P_l denote the distribution of $(X, \mathbb{1}\{Y = l\})$. Clearly, D_l is a set of n i.i.d. samples from P_l , and h_l is learning a binary calibrator with respect to P_l using binary histogram binning. The number of data-points is n and the number of bins is $B_l = \lfloor n/k_l \rfloor$ bins. We now apply the GR21 bounds on h_l . First, we verify that the condition they require is satisfied:

$$n \geq k_l \lfloor n/k_l \rfloor \geq 2B_l.$$

Thus the GR21 marginal calibration bound gives that for every $l \in [L]$, h_l satisfies

$$P \left(|P(Y = l | h_l(X)) - h_l(X)| \leq \delta + \sqrt{\frac{\log(2/\alpha_l)}{2(\lfloor n/B_l \rfloor - 1)}} \right) \geq 1 - \alpha_l.$$

The class-wise marginal calibration bound of Theorem 2 follows since $\lfloor n/B_l \rfloor = \lfloor n/\lfloor n/k_l \rfloor \rfloor \geq k_l$, and so

$$\varepsilon_l^{(1)} \geq \delta + \sqrt{\frac{\log(2/\alpha_l)}{2(\lfloor n/B_l \rfloor - 1)}}.$$

Next, the GR21 conditional calibration bound gives for every $l \in [L]$, h_l satisfies

$$P \left(\forall r \in \text{Range}(h_l), |P(Y = l | h_l(X) = r) - r| \leq \delta + \sqrt{\frac{\log(2B_l/\alpha_l)}{2(\lfloor n/B_l \rfloor - 1)}} \right) \geq 1 - \alpha_l.$$

The class-wise marginal calibration bound of Theorem 2 follows since $B_l = \lfloor n/k_l \rfloor \leq n/k_l$ and $\lfloor n/B_l \rfloor = \lfloor n/\lfloor n/k_l \rfloor \rfloor \geq k_l$, and so

$$\varepsilon_l^{(2)} \geq \delta + \sqrt{\frac{\log(2B_l/\alpha_l)}{2(\lfloor n/B_l \rfloor - 1)}}.$$

Let $k = \min_{l \in [L]} k_l$. The in-expectation ECE bound of GR21, for $p = 1$, gives for every l ,

$$\begin{aligned} \mathbb{E} [\text{binary-ECE-for-class-}l (h_l)] &\leq \sqrt{B_l/2n_l} + \delta \\ &= \sqrt{\lfloor n/k_l \rfloor / 2n} + \delta \\ &\leq \sqrt{1/2k_l} + \delta \\ &\leq \sqrt{1/2k} + \delta. \end{aligned}$$

Thus,

$$\begin{aligned} \mathbb{E} [\text{CW-ECE}(c, h)] &= \mathbb{E} \left[L^{-1} \sum_{l=1}^L \text{binary-ECE-for-class-}l (h_l) \right] \\ &\leq L^{-1} \sum_{l=1}^L (\sqrt{1/2k} + \delta) \\ &= \sqrt{1/2k} + \delta, \end{aligned}$$

as required for the in-expectation CW-ECE bound of Theorem 2. Finally, for the high probability CW-ECE bound, let $\varepsilon = \max_{l \in [L]} \varepsilon_l^{(2)}$ and $\alpha = \sum_{l=1}^L \alpha_l$. By taking a union bound over the the conditional calibration bounds for each h_l , we have, with probability $1 - \alpha$, for every $l \in [L]$ and $r \in \text{Range}(h)$,

$$|P(Y = l | c(X) = l, h(X) = r) - r| \leq \varepsilon_l^{(2)} \leq \varepsilon.$$

Thus, with probability $1 - \alpha$,

$$\text{CW-ECE}(c, h) = L^{-1} \sum_{l=1}^L \mathbb{E} |P(Y = l | h_l(X)) - h_l(X)| \leq \varepsilon.$$

This proves the high-probability bound for the CW-ECE. \square

D Additional experimental details and results for Sections 1 and 2

This section presents further experimental details and results to supplement those presented in Sections 1 and 2 of the main paper. Appendix D.1 discusses the COVTYPE-7 dataset. Appendix D.2 discusses the CIFAR datasets. In Appendix D.2, we also define a top-label version of the maximum calibration error (MCE) metric [Guo et al., 2017, Naeini et al., 2015], and show results on the CIFAR datasets for this metric. Overall, we find that top-label HB typically performs better than temperature scaling for MCE.

D.1 Top-label calibration of COVTYPE-7

We present additional details and results for the top-label HB experiment of Section 2.2. The base classifier is an RF learnt using `sklearn.ensemble import RandomForestClassifier` with default parameters. The base RF is a nearly continuous base model since most predictions are unique. Thus, we need to use binning to make reliability diagrams, validity plots, and perform ECE estimation, for the base model. To have a fair comparison, instead of having a fixed binning scheme to assess the base model, the binning scheme was decided based on the unique predictions of top-label HB. Thus for every l , and $r \in \text{Range}(h_l)$, the bins are defined as $\{x : c(x) = l, h_l(x) = r\}$. Due to this, while the base model in Figures 3a and 3b are the same, the reliability diagrams and validity plots in orange are different. As can be seen in the bar plots in Figure 3, the ECE estimation is not affected significantly.

When $k = 100$, the total number of bins that were chosen by Algorithm 1 was 403, which is roughly 57.6 bins per class. The choice of $B = 50$ for the fixed bins per class experiment was made on this basis.

Figure 11 supplements Figure 3 in the main paper by presenting reliability diagrams and validity plots of top-label HB for all classes. Figure 11a presents the plots with adaptive number of bins per class (Algorithm 1), and Figure 11b presents these for fixed number of bins per class. We make the following observations.

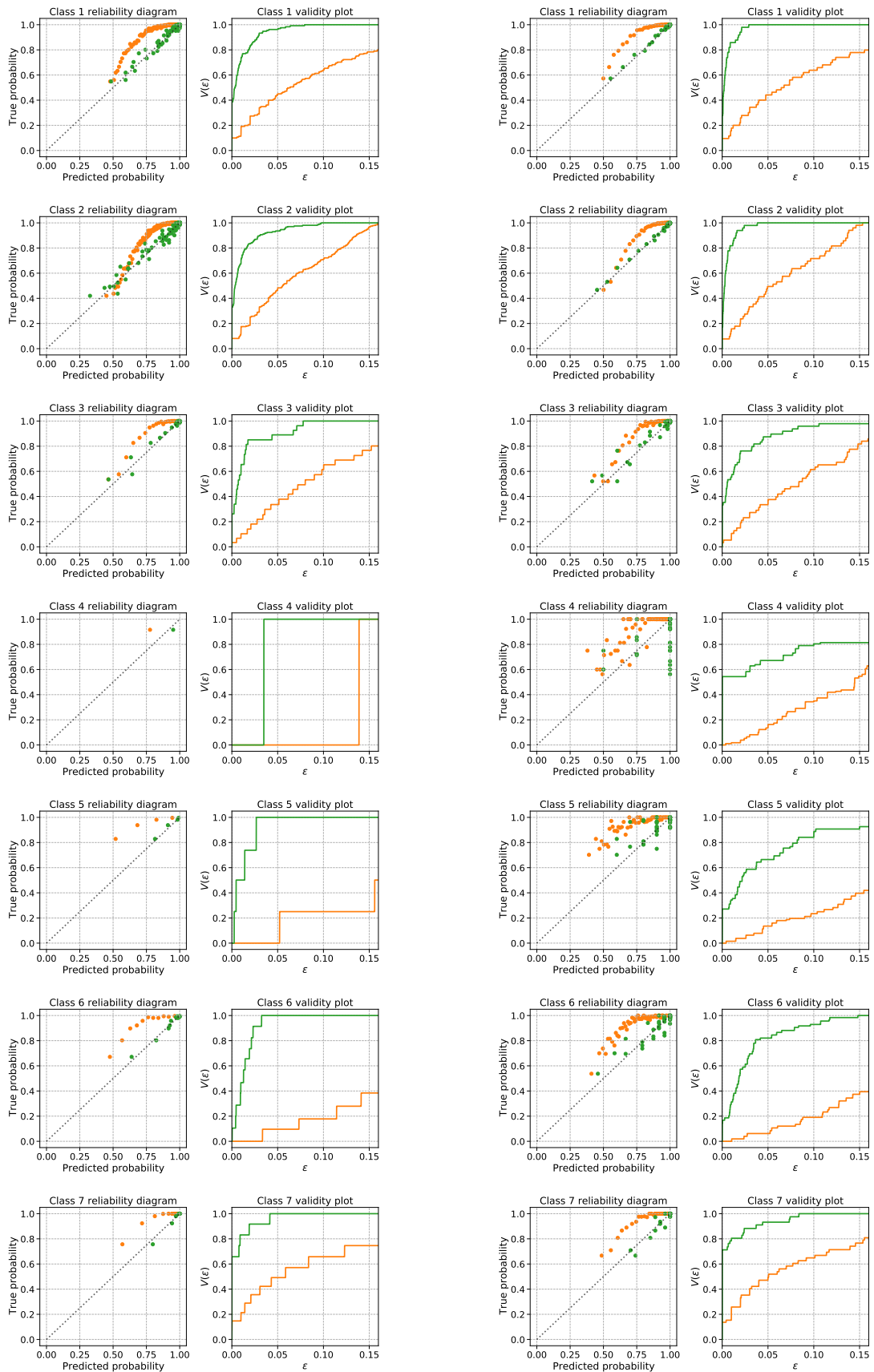
- (a) For every class $l \in [L]$, the RF is overconfident. This may seem surprising at first since we generally expect that models may be overconfident for certain classes and underconfident for others. However, note that all our plots assess top-label calibration, that is, we are assessing the predicted and true probabilities of only the predicted class. It is possible that a model is overconfident for every class whenever that class is predicted to be the top-label.
- (b) For the most likely classes, namely classes 1 and 2, the number of bins in the adaptive case is higher than 50. Fewer bins leads to better calibration (at the cost of sharpness). This can be verified through the validity plots for classes 1 and 2 — the validity plots in the fixed bins case is slightly ‘above’ the validity plot in the adaptive bin case. However both validity plots are quite similar.
- (c) The opposite is true for the least likely classes, namely classes 4, 5, 6. The validity plot in the fixed bins case is ‘below’ the validity plot in the adaptive bins case, indicating higher TL-ECE in the fixed bins case. The difference between the validity plots is high. Thus if a fixed number of bins per class is pre-decided, the performance for the least likely classes significantly suffers.

Based on these observations, we recommend adaptively choosing the number of bins per class, as done by Algorithm 1.

D.2 Top-label calibration of CIFAR-10 and CIFAR-100

We present additional details and results for the top-label HB experiment of Sections 1, 2.3, and 2.4. All our base models were pre-trained deep net models generated by Mukhoti et al. [2020]; further details for the training can be found at the repository located at https://github.com/torrvision/focal_calibration. We also used their code to learn the temperature scaling parameter T . There was no additional tuning required to generate the results.

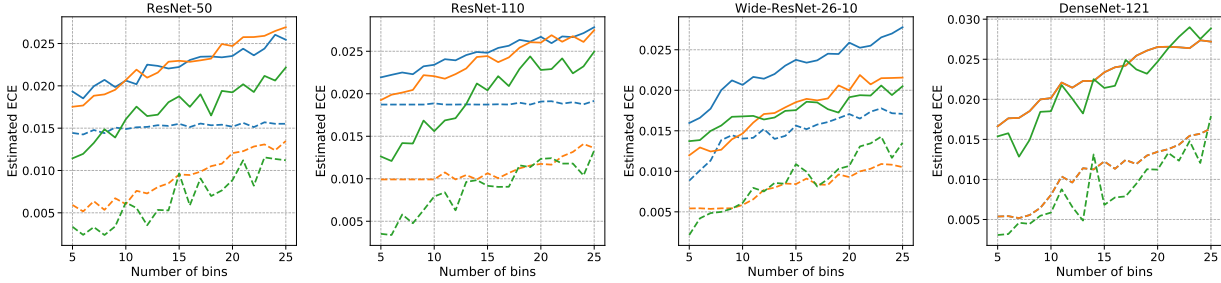
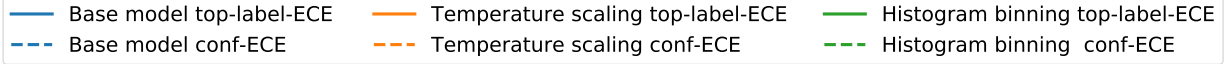
The conf-ECE and TL-ECE estimation for the base model and temperature scaling was done using fixed-width bins $[0, 1/B), [1/B, 2/B), \dots [1 - 1/B, 1]$. Plugin estimates of the ECE were used, same as Guo



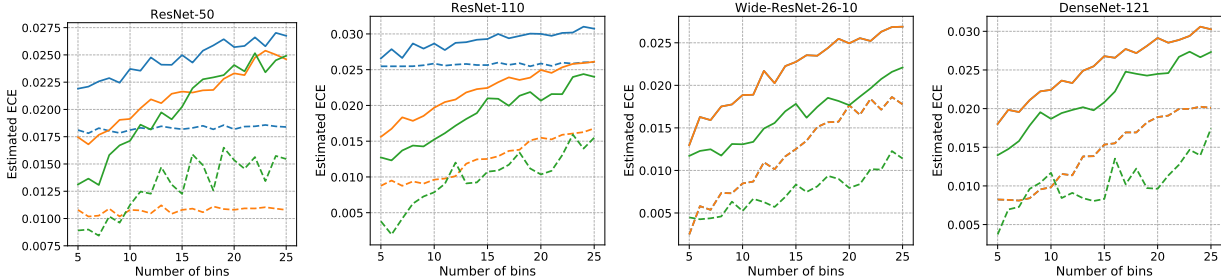
(a) Top-label HB with $k = 100$ points per bin.

(b) Top-label HB with $B = 50$ bins per class.

Figure 11: Top-label histogram binning (HB) calibrates a miscalibrated random-forest on the class imbalanced COVTYPE-7 dataset. For the less likely classes (4, 5, and 6), the left column is better calibrated than the right column. Similar observations are made on other datasets, and so we recommend adaptively choosing a different number of bins per class, as Algorithm 1 does.



(a) Optimized using focal loss.



(b) Optimized using Brier score.

Figure 12: Conf-ECE and TL-ECE of histogram binning and temperature scaling with deep nets on CIFAR-10. When assessed with respect to TL-ECE (solid lines in all plots), histogram binning is always comparable to temperature scaling, and often performs better.

et al. [2017]. The TL-ECE estimation for top-label HB did not use further binning since HB is already a discrete output method (due to Jensen’s inequality, any further binning will only decrease the ECE estimate). The conf-ECE estimation for top-label HB is trickier since $\text{Range}(h_l)$ is different for different l , and thus the averaging across bins cannot be done unless we further define bins based on fixed-width binning. We observed in our experiments that fixed-width binning decreased the conf-ECE of top-label HB. To have a fairer comparison, instead of fixed-width binning, we merged the k ’th bins across all classes for estimating conf-ECE. That is, for a given k , we considered the bins across classes corresponding to the k/B and $(k+1)/B$ quantiles on calibration data, and computed the average confidence and accuracy for the test points that belong to these bins (across all predicted top-labels).

Figures 12 presents results of our experiments on additional deep net architectures with CIFAR-10, to supplement Figure 4 in the main paper. Figure 13 presents results with CIFAR-100. The observations are very similar to those presented in the main paper.

In some plots, such as the Wide-Resnet-26-10 plot in Figure 4b and Figure 12b, the blue base model line and the orange temperature scaling line intersect. This is not surprising; it occurs since the optimal temperature on the calibration data was learnt to be $T = 1$, which corresponds to not changing the base model at all. Even in such cases when temperature scaling changes the base model by a little, or not at all, top-label HB shows improved performance.

Next, we discuss results with respect to conditional calibration, or the maximum calibration error (MCE). Guo et al. [2017] defined MCE with respect to confidence calibration, as follows:

$$\text{conf-MCE}(c, h) := \sup_{r \in \text{Range}(h)} |P(Y = c(X) \mid h(X) = r) - r|. \quad (19)$$

Conf-MCE suffers from the same issue illustrated in Figure 1. In Figure 1c, we looked at the reliability diagram within two bins. These indicate two of the values over which the supremum is taken in equation (19):

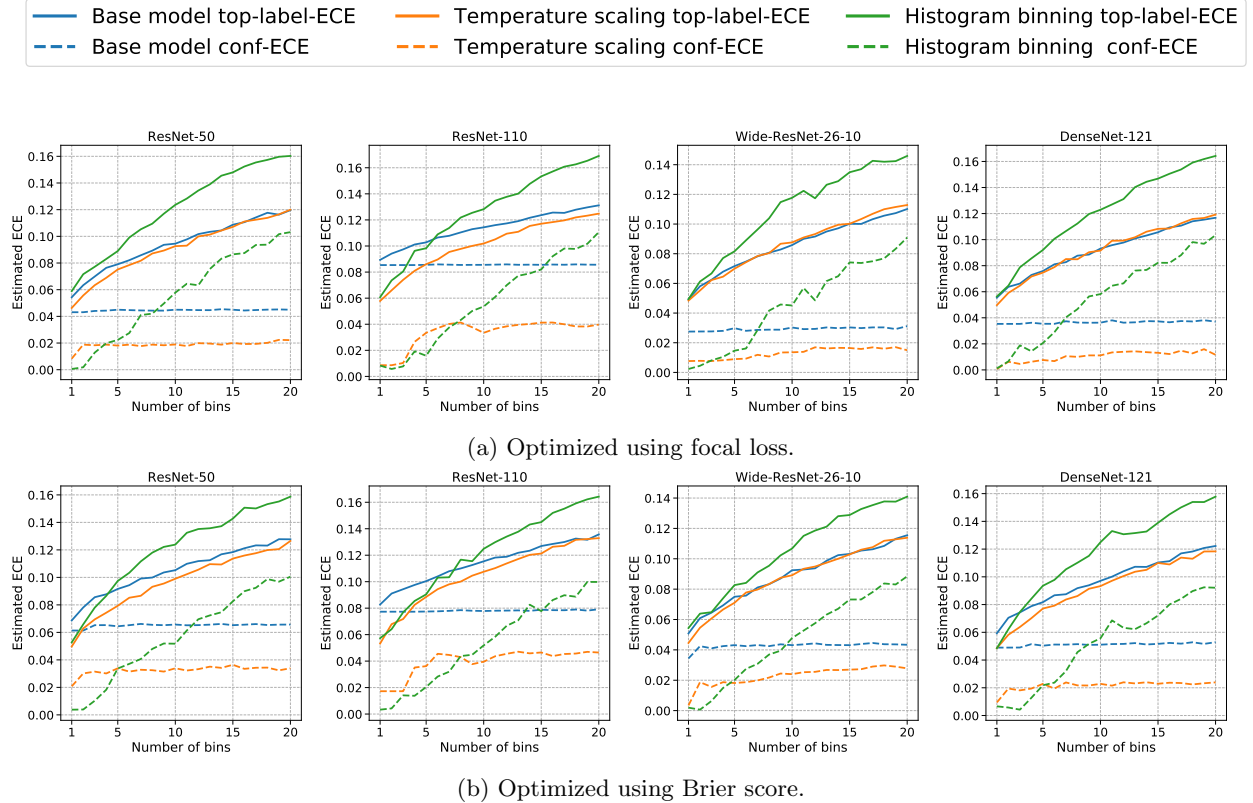


Figure 13: Conf-ECE and TL-ECE of histogram binning and temperature scaling with deep nets on CIFAR-100. When assessed with respect to TL-ECE (solid lines in all plots), temperature scaling typically performs better than histogram binning. In fact, the performance of histogram binning is often worse than even the base model.

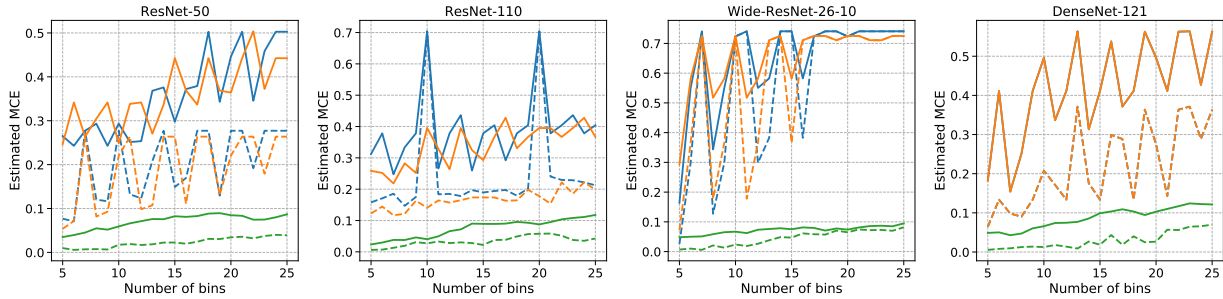
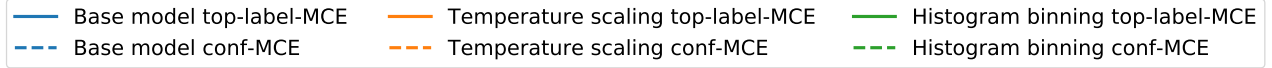
these are the Y-axis distances between the \star markers and the $X = Y$ line for bins 6 and 10 (both are less than 0.02). On the other hand, the effective ‘maximum’ miscalibration for bin 6 is roughly 0.15 (for class 1), and roughly 0.045 (for class 4), and the maximum should be taken with respect to these values across all bins. To remedy the underestimation of the effective MCE, we can consider the top-label-MCE, defined as follows:

$$\text{TL-MCE}(c, h) := \max_{l \in [L]} \sup_{r \in \text{Range}(h)} |P(Y = l \mid c(X) = l, h(X) = r) - r|. \quad (20)$$

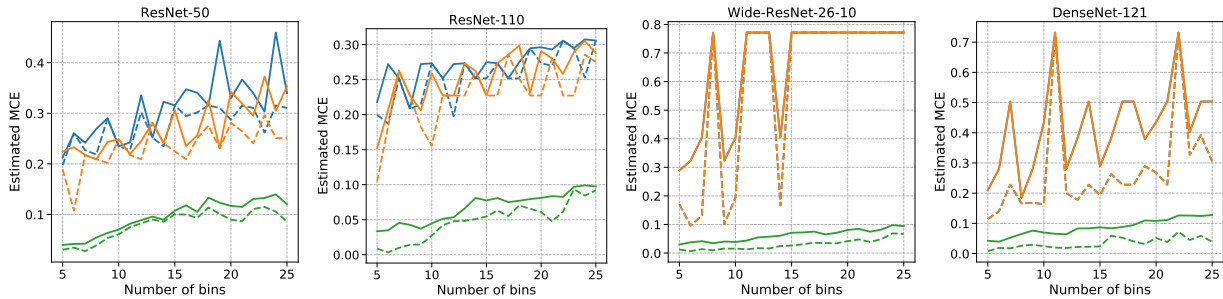
Interpreted in words, the TL-MCE assesses the maximum deviation between the predicted and true probabilities across all predictions and all classes. Following the same argument as in the proof of Proposition 1, it can be shown that for any c, h , $\text{conf-MCE}(c, h) \leq \text{TL-MCE}(c, h)$. The TL-MCE is closely related to conditional top-label calibration (Definition 1b). Clearly, an algorithm is (ε, α) -conditionally top-label calibrated if and only if for every distribution P , $P(\text{TL-MCE}(c, h) \leq \varepsilon) \geq 1 - \alpha$. Thus the conditional top-label calibration guarantee of Theorem 1 implies a high probability bound on the TL-MCE as well.

Since top-label HB ensures that each bin has roughly k points, we expect that reasonable levels of calibration will be achieved across all bins. Consequently, we expect the MCE of top-label HB to be relatively small. This is confirmed empirically in the upcoming results.

Figure 14 shows conf-MCE and TL-MCE estimates of deep nets on CIFAR-10 for top-label HB, temperature scaling, and the base model. In Section 2.3, we had observed that top-label HB shows a slight but consistent improvement over temperature scaling for TL-ECE. For TL-MCE, top-label HB shows a *large and consistent* improvement over temperature scaling across all architectures. Notice that for $B = 15$, the TL-MCE of temperature scaling is always larger than 0.2. On the other hand, across different deep net architectures, loss functions, and numbers of bins, the TL-MCE of top-label HB is always below 0.1. This is



(a) Optimized using focal loss.

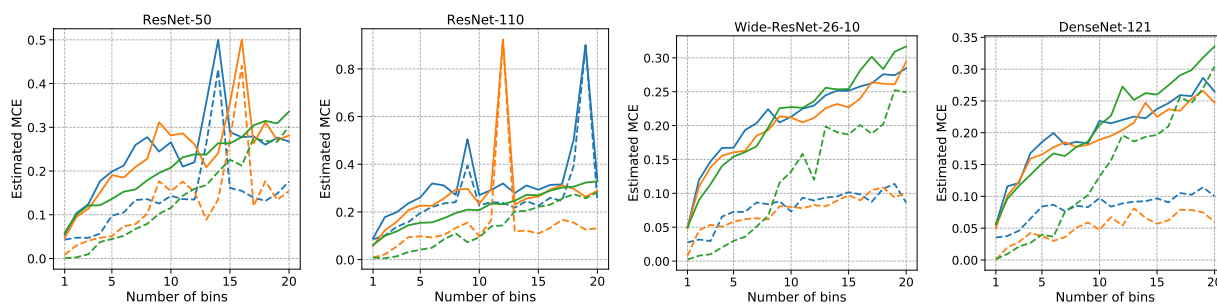
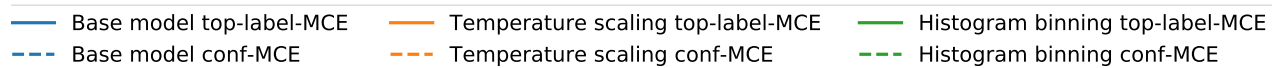


(b) Optimized using Brier score.

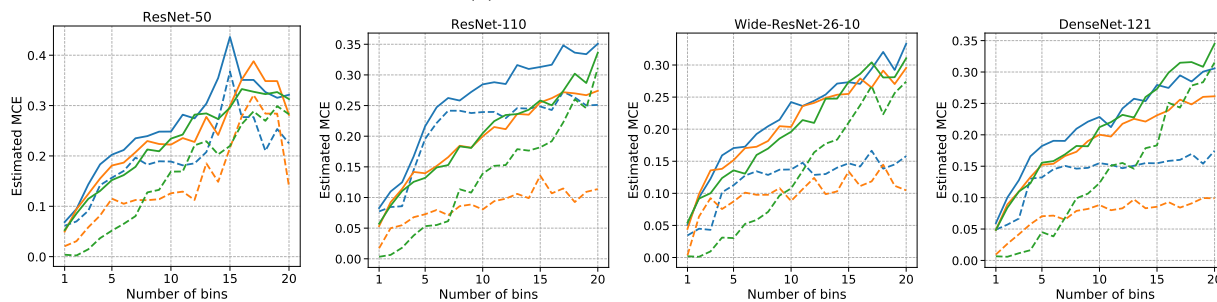
Figure 14: Conf-MCE and TL-MCE of top-label histogram binning (HB) and temperature scaling (TS) with deep nets on CIFAR-10. HB shows multi-fold improvements over TS across architectures, loss functions, and numbers of bins. Unlike TS, the MCE is stable across different numbers of bins. For the Wide-ResNet-26-10 model optimized with Brier score, the base model has an estimated TL-MCE as well as conf-MCE of around 0.77. While TS did not recalibrate this model at all ($T = 1$), top-label HB achieves a TL-MCE of around 0.065, more than a 10-fold improvement.

a powerful empirical result: for *every* test point $x \in \mathcal{X}$, the prediction $h(x)$ provided by top-label HB is at most 0.1 away from the true probability $\mathbb{E}[Y = c(x) \mid c(X) = c(x), h(X) = h(x)]$.

Figure 15 shows conf-MCE and TL-MCE estimates of deep nets on CIFAR-100 for top-label HB, temperature scaling, and the base model. In Section 2.4, we had observed that temperature scaling performs better than top-label HB when assessed with respect to TL-ECE. For TL-MCE, we observe that the performance of top-label HB and temperature scaling is quite comparable. For $B = 15$, the TL-MCE of top-label HB is always below 0.3. Further, the MCE of temperature scaling is quite unstable as the number of bins changes, the most instabilities occurring for the ResNet-50 and ResNet-100 plots with focal loss.



(a) Optimized using focal loss.



(b) Optimized using Brier score.

Figure 15: Conf-MCE and TL-MCE of top-label histogram binning (HB) and temperature scaling (TS) with deep nets on CIFAR-100. The TL-MCE of HB, TS, and the base model are comparable, but HB is more stable across different numbers of bins.